ANKRD9 IS A METABOLICALLY-CONTROLLED REGULATOR OF IMPDH2 ABUNDANCE AND MACRO-ASSEMBLY

by
Dawn Hayward

A dissertation submitted to The Johns Hopkins University in conformity with the requirements of the degree of Doctor of Philosophy

Baltimore, Maryland
April 2019

ABSTRACT

Members of a large family of Ankyrin Repeat Domains proteins (ANKRD) regulate numerous cellular processes by binding and changing properties of specific protein targets. We show that interactions with a target protein and the functional outcomes can be markedly altered by cells' metabolic state. ANKRD9 facilitates degradation of inosine monophosphate dehydrogenase 2 (IMPDH2), the rate-limiting enzyme in GTP biosynthesis. Under basal conditions ANKRD9 is largely segregated from the cytosolic IMPDH2 by binding to vesicles. Upon nutrient limitation, ANKRD9 loses association with vesicles and assembles with IMPDH2 into rod-like structures, in which IMPDH2 is stable. Inhibition of IMPDH2 with Ribavirin favors ANKRD9 binding to rods. The IMPDH2/ANKRD9 assembly is reversed by guanosine, which restores association of ANKRD9 with vesicles. The conserved $Cys^{109}Cys^{110}$ motif in ANKRD9 is required for the vesicles-to-rods transition as well as binding and regulation of IMPDH2. ANKRD9 knockdown increases IMPDH2 levels and prevents formation of IMPDH2 rods upon nutrient limitation. Thus, the status of guanosine pools affects the mode of ANKRD9 action towards IMPDH2.

Advisor: Dr. Svetlana Lutsenko, Department of Physiology, Johns Hopkins University School of Medicine

Second reader: Dr. Carolyn Machamer, Department of Cell Biology, Johns Hopkins University School of Medicine

TABLE OF CONTENTS

Intended to be blank

List of Figures

Figure **Page**

Chapter 1: Introduction

Section 1.1: Ankyrin Repeat domain containing proteins

Section 1.2: Inosine monophosphate dehydrogenases

Chapter 1: Introduction

Section 1.1: Ankyrin Repeat domain containing proteins

Introduction to ANKRD9 and ankyrin domain-containing (ANKRD) proteins

ANKRD9 (ankyrin-domain containing protein 9) is a 35 kDa protein with at least one predicted ankyrin repeat. Typically, ankyrin repeats are involved in protein-protein interactions which are essential for a variety of cellular processes. While there are around 60 ANKRD proteins that are small, soluble adapter proteins, the majority of ankyrin repeats exist as a domain of several repeats within a larger protein. This chapter describes the types of repeats found in proteins (Section 1.1.1), the discovery and structure of ankyrin repeats (Section 1.1.2) and finally a selection of proteins that contain ankyrin repeats (Section 1.1.3). These examples illustrate the importance of generating a surface for protein-protein interaction and put into context the relationship between ANKRD9 and its partner IMPDH2, described in Section 1.2. In our studies we have shown that ANKRD9 stabilizes IMPDH2 macro-assembly in the form of rods and that this structure may serve to protect IMPDH2 from degradation by ANKRD9.

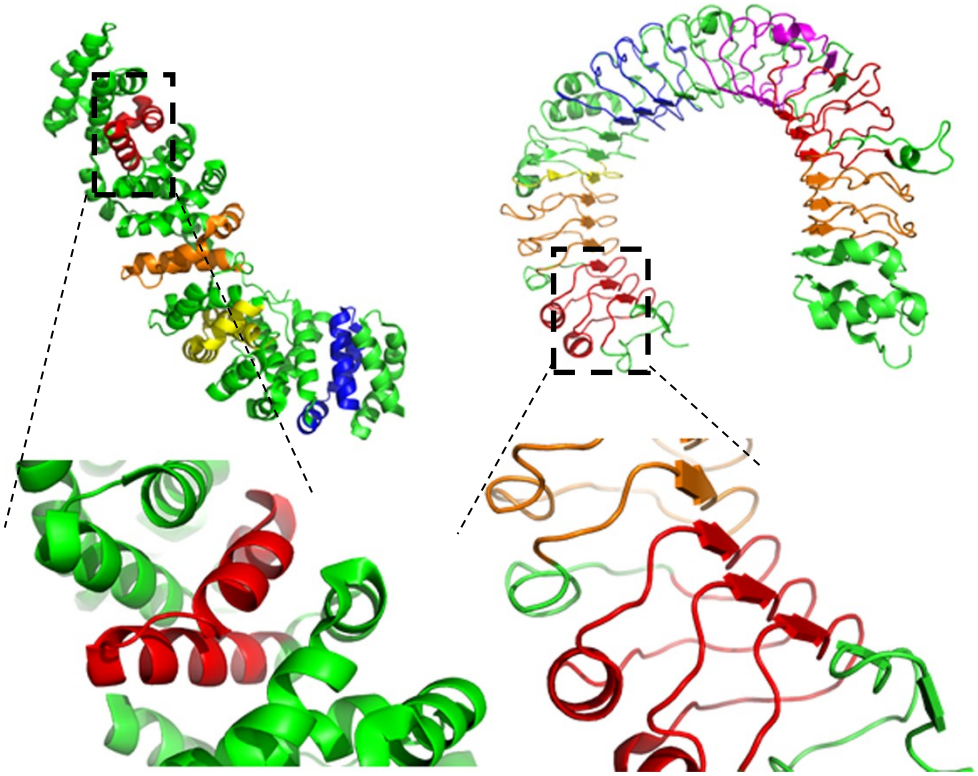

Figure 1: Repeats found in different proteins. On the top left is β-catenin (PDB 1JDH (1)) with each color representing an armadillo repeat, a close-up view is shown on the bottom left. On the top right is Toll-like Receptor 3 (PDB 2A0Z (2)) with each color representing a leucine rich repeat, a close- up view is shown on the bottom. Ankyrin repeats rank among these as the most used repeats in proteins serving a variety of functions.

Section 1.1.1: Types of structural repeats in proteins

Ankyrin domains are among the most used repeats in proteins

Tandem repeats in proteins are widespread with several appearing most often. These include ankyrin repeats, leucine rich sequences, and tetratricopeptide, armadillo and HEAT repeats (3). These repeats are described as follows: leucine-rich repeats make for a greasy, hydrophobic surface; tetratricopeptide and armadillo repeats each form a superhelical structure or solenoid and HEAT (Huntingin-elongation factor 3 (EF3), protein phosphatase 2A (PP2A) subunit, PI3-kinase TOR1) repeats form short, flexible helices (3,4) (Figure 1). Ankyrin repeats (AR) are usually around 30-34 amino acids long and consist of both hydrophobic and hydrophilic residues. Proteins containing several AR (as many as 24 repeats can be present) typically form curved solenoid structures and participate in processes ranging from cell cycle regulation to signaling. The association of AR-containing proteins with inherited and sporadic disease underscores their importance and need to be explored (5-8). A common thread throughout these repeats is the significance of secondary structure. Many of the primary 'consensus' sequences for these repeats are guidelines to the secondary fold rather than indicators of absolute sequence requirement. For example: hydrophobic residues have been replaced for more hydrophilic residues to have better access to solvent (3). Although the repeats in proteins are widespread, oftentimes their function is not fully understood.

Uniqueness of ankyrin repeats compared to others

Ankyrin repeats are unique in several aspects. In addition to proteins containing several ankyrin repeats as a well-defined part of their structure, there are over 60 'orphan' proteins that contain one or more ankyrin repeats, many of which have no defined function.

A role in autophagy has been described for ANKRD49 and a role in membrane binding and cardiac function has been described for ANKRD1 (9,10). Additionally, while other repeats participate mainly in protein-protein interaction, ankyrin repeats have been recently shown to mediate binding of proteins to lipids and sugars as well as small molecules as in TRPV4, described in Section 1.1.3 (3,11). Lastly, most of the repeats discussed earlier in this chapter are composed of alpha helices only and can pack to form higher order solenoid structures. Ankyrin repeats form a helix-turn-helix structure where as many as 24 repeats can stack to form a surface for protein-protein interactions, as observed in the human ankyrin protein (12). These features make ankyrin repeats versatile and somewhat elusive in determining their exact function in a given cellular state.

Section 1.1.2. The discovery and structure of ankyrin repeats

The helix-turn-helix nature of ankyrin repeats forms a concave structure

Ankyrin repeats find their history from yeast and fly studies. The repeat was discovered as part of the cell cycle complex Swi6/Cdc10 in yeast as well as in *Drosophila* protein Notch (3,5). Human ankyrin was then shown to have homology to the *Drosophila* protein and to contain 24 ankyrin repeats. The structure of 12 ankyrin repeat stacks (repeats 13-24) from human ankyrin was determined and revealed the presence of a membrane binding domain, spectrin binding domain and a death domain (12). Additionally, the structure identified a consensus sequence Threonine-Proline-Leucine-Histidine (TPLH) that marks the beginning of the first alpha helix of the repeat that occurs in every repeat in this report and the repeat in ANKRD9 (Figure 2).

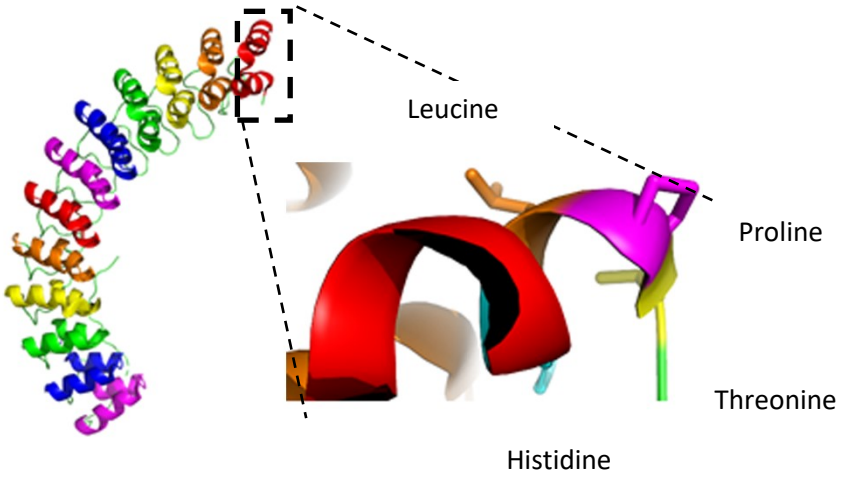

Figure 2: Ankyrin repeats in human Ankyrin. A 12 ankyrin stack is depicted on the left and a close-up view on the right. Each color on the left depicts one ankyrin repeat. The TPLH motif is boxed and is as follows. T:yellow, P: magenta, L:orange, H: cyan. Adapted from, (12), PDB 1N11.

The threonine residue identifies the beginning of both the alpha helix and the start of an ankyrin repeat (12). These residues were conserved in the 12 repeats solved in this structure. The secondary structure also revealed a so-called 'ankyrin groove' which has since been defined as the first alpha helix and β-hairpin of a single repeat, forming an L-shape (12). Several ankyrin repeats together (Figure 2) form a concave structure with the helices on the outside and the β-hairpin turns on the inside. Within one repeat, stability is afforded by a group of small non-polar residues making up the alpha helices where longer range contacts are made by a hydrogen bond network which partially consists of aromatic residues between the helices. Smaller, flexible residues such as glycine and alanine also make up this region to allow for the turns. The presence of more than one repeat in ankyrin proteins could be explained by the observation that one repeat in solution does not properly fold unless another repeat is present (13).

Binding of ankyrin repeats to other proteins

ANKRDs bind ankyrin repeats in other proteins primarily through the concave fold discussed above. The repeats may modulate catalytic activity, mediate interactions between proteins, increase protein stability, regulate protein expression and targeting and can even be used for drug targeting (14-19). The structures of ankyrin repeats from several proteins have been solved; these structures provide direct evidence for protein-protein interactions at the alpha helices that make up the backbone of the repeats (20-22). Additionally, software has been developed to predict such interactions within and between proteins containing these

repeats (23). Interestingly, while much of the interactions occur on the helix folds, the beta hairpin loops were shown to function as dimerization domains (24). In our work described in Chapter 2 interactions between ANKRD9 and IMPDH2 occurred specifically in the loop regions of ANKRD9.

Section 1.1.3: Important ankyrin repeat containing proteins

TRPV channels contain ankyrin repeats involved in disease and small molecule binding

Ankyrin repeats do not typically recognize a particular set of residues (6). Rather, their stacking generates a platform upon which proteins bind and carry out essential functions. This emphasis on secondary structure is especially important when considering the function of proteins that contain these repeats. In addition to the cytoskeletal ankyrin itself, the most well-known proteins that contain ankyrin repeats are the Transient Receptor Potential channels or TRPV (11,25,26). These cation channels have several subfamilies including TRPA channels, whose intracellular domain consists of several ankyrin repeats (25). These channels respond to a variety of stimuli including stress, cell swelling, heat and to certain chemicals like arachidonic acid and ligands like 4α-phorbol-12,13-didecanoate (11). Mutations in these channels can lead to many diseases, including Charcot-Marie-Tooth disease, with some mutations occurring within the ankyrin repeats of these proteins (11,25).

Studies examining channel activity have found that the ankyrin repeats modulate many properties including channel sensitivity. In fact, it was shown that an ankyrin repeat within TRPV4 directly and specifically binds phosphatidylinositol-4,5-bisphosphate ($PI(4,5)P_2$) which then blocks channel activity; gain-of-function mutations specifically prevent binding of PI(4,5)P2 to the ankyrin repeat (11). This finding followed two previous

studies where ATP was also shown to bind to the ankyrin repeats of TRPV4. This binding stabilized the ankyrin fold and also modulated channel activity (25,26). The ankyrin repeat serves to significantly modulate channel activity of TRPV4 owing to its large surface for protein-protein interactions. It is also interesting that ATP binding stabilizes the ankyrin fold, indicating that one metabolite may regulate these types of repeats. In Chapter 2 we show that GTP may regulate the macromolecular assembly of ANKRD9.

Bcl-3 is a signaling protein whose ankyrin repeats aid in NF-κB function

Another important ankyrin-domain containing protein is Bcl-3, which is involved in NF-κB signaling. NF-κB is a transcription factor whose translocation to the nucleus is inhibited by IκBα, or inhibitor of NF-κB, which masks NF-κB's nuclear localization signal (27). Bcl-3 is a member of the IκB family but is nucleoplasmic and serves as a co-activator once NF-κB signaling pathways are activated to allow translocation to the nucleus (28). Both Bcl-3 and IκB have ankyrin repeats, so it was intriguing that they essentially carried out opposing functions. The crystal structure of the ankyrin domain of Bcl-3 revealed that a seventh ankyrin repeat was present in Bcl-3 (there are 6 in IκB) and several residues in this repeat could not bind the nuclear localization signal of NF-κB like IκB could (27). In addition, Bcl-3 forms a stable complex with DNA whereas IκB cannot, owing to an exposed basic surface in the seventh Bcl-3 ankyrin repeat as revealed by modeling studies (27). This example shows that ankyrin repeats can influence entire cell signaling networks, and the mere presence of ankyrin repeats in two different proteins does not necessarily translate to having similar functions.

Tankyrase contains ankyrin repeats responsible for substrate binding

Tankyrase 1(PARP5A or ARTD5) and 2, are enzymes involved in the addition of ADP-ribosyl moieties to target proteins. Tankyrase 1 and 2 belong to the poly (ADP-ribose) polymerase (PARP) enzymes (29). Addition of ADP-ribose has several consequences including subsequent ubiquitylation and degradation, however when a single ADP-ribose is added other signaling consequences ensue. What is unique about these proteins is that Tankyrase 1 and 2 in particular have 24 ankyrin repeats called the ankyrin repeat cluster or ARC in addition to a catalytic site and several other domains (29). For Tankyrase 1, several of its ankyrin repeats are responsible for substrate binding to allow the PARP enzymatic domain to add the ADP-ribose modification to its target. One such substrate is AXIN which is involved in the WNT signaling pathway where Tankyrase 1 binds AXIN through ARC2,4,5 and 1 which also causes Tankyrase 1 dimerization (29). This is important as it shows how ankyrin repeats can influence conformation. In Chapter 2 we describe how ANKRD9 binds to and stabilizes IMPDH2 rod macroassembly.

Tankyrase also has roles in telomere extension. Tankyrase-mediated ADP-ribosylation of TRF1(telomeric repeat binding factor 1) prevents it from blocking access to the telomere. Furthermore, Tankyrase is involved in insulin-dependent glucose uptake (30). It has been recently shown that in skeletal muscle Tankyrase 1 inhibition or downregulation is associated with a decrease in abundance of several glucose transporters including insulin-responsive GLUT4. Reversal of the Tankyrase effect on GLUT4 stability was achieved by blocking the proteasome (30). This example shows that ankyrin repeats can be responsible for differing downstream functions similar to Bcl-3 and IκB.

Phospholipases have diverse functions and contain ankyrin repeats involved in oligomerization

Phospholipases A_2 comprise an additional family of ankyrin-containing proteins (31-33). Specifically, iPLA$_2$β has 8 ankyrin repeats that are involved in the oligomer formation and activity of this enzyme (32). iPLA$_2$β is a calcium independent phospholipase A, which has lysophospholipase activity. In addition to the ankyrin repeats, iPLA$_2$β has a nucleotide binding motif, an N-terminal caspase-3 site and a nuclear localization sequence (33). The ankyrin repeats have been shown to influence oligomeric formation where iPLA$_2$β subunits interact via their ankyrin repeats. In fact, the enzyme with ankyrin repeat mutations was reported inactive (32). Additionally the nucleotide binding region of iPLA$_2$β has been shown to bind ATP, similar to the TRPV4 channel, and this binding promotes stabilization of oligomer (34). That oligomeric formation requires ankyrin repeats points to their extensive involvement in varied and complex protein-protein interactions where structure informs function. Interestingly, ankyrin repeats are only found in this specific phospholipase. Other phospholipases, including iPLA$_2$γ, which is implicated in mitochondrial function and fat utilization, and iPLA$_2$ζ, which plays a role in triacylglyceride deposition, do not have ankyrin repeats(33).These phospholipases have not been shown to oligomerize which may be the reason why they do not contain ankyrin repeats.

iPLA$_2$β is involved in a host of processes, including membrane remodeling, cell proliferation, bone formation and male fertility (33,35,36). A common theme through these seemingly disparate processes is the products of iPLA$_2$β enzymatic activity, which are responsible for the downstream effects. For example, in membrane remodeling the

lysophospholipid acceptors generated as products are proposed to help arachidonic acid integration into phospholipids for eventual incorporation into the phospholipid bilayer (33). During cell proliferation again the iPLA$_2$β products are proposed as responsible for activating the transcription of certain genes for cell division. Overall, ankyrin repeats not only provide necessary surfaces for protein-protein interaction but also are required for activity. This underscores the need for multiple ankyrin repeats to carry out different activities and ankyrin containing proteins typically have several repeats.

Conclusions on ankyrin domain containing proteins

The above examples of important classes of proteins containing ankyrin repeats highlight protein-protein interactions as the main driver of varied repeat functions from pain sensing channels to NF-κB signaling to phospholipase activity. While there is some conservation in the sequence of these repeats, it is their secondary structure that dictates function. Throughout evolution many residues have been replaced for more favorable ones, yet the overall fold has been preserved. Additionally, these different classes highlight the importance of multiple (up to 24) repeats. A single repeat alone is generally unfolded and lacks its characteristic helix-hairpin-helix structure (13).

In addition to proteins that have ankyrin repeats as a part of the structure, there are small proteins composed of ankyrin repeats alone without enzymatic activity. The function and mechanism behind their cellular activities are often not well understood. Indeed, ankyrin domain containing proteins such as ANKRD9 studied here may not have enzymatic activity or multiple different domains but instead are utilized by other proteins lacking ankyrin repeats for their functionality. This could be helpful for separating different functions

spatially or temporally. Also, association with one ankyrin domain containing protein or another could be useful under different circumstances.

Section 1.1.4: ANKRD9 identification and roles

ANKRD9 has several varied roles

ANKRD9, or ankyrin-domain containing protein 9, is a small 35 kDa protein with one reported ankyrin repeat occurring at residues 32-203, however according to the consensus sequence described in Section 1.1.2 the ankyrin repeat occurs at amino acid residues 195-216. Additionally, the secondary structure, shown in Figure 10a, consists of mostly helix-turn-helix repeats which is the ankyrin fold so there may be more although they may not have the canonical sequence. A structural model of ANKRD9 shows that the protein is made up of helix-hairpin-helices (see Figure 10a in Chapter 2, Section 2.3). ANKRD9 is predicted to have 5 splice variants and 4 exons; all splice variants encode the ANKRD9 protein. ANKRD9 expression is ubiquitous in most tissues, with slightly elevated expression in skeletal muscle and the colon (https://www.genecards.org/cgibin/carddisp.pl?gene=ANKRD9&keywords=ANKRD9), it is not known whether isoforms are expressed in different tissues. ANKRD9 is one of at least 60 ankyrin-domain containing proteins where roles have only been assigned to a few of them, including ANKRD49 with a reported role in autophagy (9).

ANKRD9's role in copper homeostasis

In our laboratory ANKRD9 was initially discovered as a regulator of copper homeostasis. In a genome-wide RNAi screen, 21,360 genes were knocked down individually

in HeLa cells using siRNA and cellular metal levels were analyzed by ICP-MS (inductively coupled plasma mass spectrometry) to determine metal content changes. Nine elements were tested, including selenium, copper, phosphorus, magnesium, potassium, cadmium, manganese, iron and zinc. Normalization and secondary screens narrowed the list to genes that altered copper levels to a significant degree. ANKRD9 knockdown in HeLa cells increased copper levels specifically and significantly (37). ANKRD9 had a z-score of 7.18, which was similar to z-score of protein with well-established roles in copper metabolism. Further experiments confirmed the role of ANKRD9 in regulation of copper uptake and possible role in glycosylation of important copper proteins CTR1 and ATP7A (see (38,39) for a review of both proteins), but the mechanism remains under investigation.

.

ANKRD9's role in lipid metabolism

There are three additional papers concerning the role of ANKRD9. The first published study implicated ANKRD9 in lipid metabolism in the chicken (40). Authors initially compared sequences of ANKRD9 in human, mouse, chicken and zebrafish; compared to human ANKRD9 there is 85%, 70% and 63% sequence identity, respectively. Additional characterization identified that ANKRD9 was most similar to the ankyrin binding domain of Calcium independent phospholipase A_2, discussed in Section 1.1.3. ANKRD9 has no signal peptide or transmembrane domain. While the human ANKRD9 is 317 amino acids and 35 kDa the chicken ANKRD9 is 292 amino acids and 32 kDa and is expressed in the heart, muscle, brain and liver. A single ankyrin repeat was also identified from the multiple sequence alignment, spanning residues 31-203 in human ANKRD9 (40).

To investigate the role of ANKRD9 in lipid metabolism authors used a riboflavin-deficient strain of chicken (rd/rd). Fatty acid oxidation (FAO) requires riboflavin as a cofactor for acyl-CoA dehydrogenase in the first step where Palmitoyl-CoA is converted to *trans*-Δ^2- Enoyl-CoA and eventually Acetyl Co-A; embryonic development in the chicken uses FAO. Consequences of riboflavin deficiency include lipid accumulation, increases in genes promoting lipid storage such as PPARγ and adipophilin as well as loss of carbohydrate reserves; the riboflavin deficient strain is a model for lipid metabolic perturbations.

At embryonic day 13 in rd/rd chickens ANKRD9 mRNA levels were increased by about 30-fold. This suggests that higher lipid content occurring with riboflavin deficiency contributes to higher ANKRD9 levels; chickens past embryonic day 13 without riboflavin do not survive. Adding thyroid hormone (T_3) to the diet, which decreases body fat and triglyceride content and is similar to reversing the riboflavin-deficient effect, decreased ANKRD9 mRNA levels. This is consistent with the idea that higher lipid content increases ANKRD9 levels.

To further explore the metabolic changes associated with fluctuating ANKRD9 levels the authors used a fasting-refeeding model. In this model, normal animals were either fully fed, fasted for 16, 24 and 48 hours or fed for 24 hours following a 48 hour fast. They found that ANKRD9 mRNA levels increased about 7-fold in the last scenario, i.e. upon feeding after fasting. As refeeding is similar to having a lowered amount of fatty acid oxidation, which occurs in the riboflavin-deficient model, this upregulation of ANKRD9 suggests that it plays a specific role in regulating fatty acid oxidation. The authors lastly showed that when overexpressed in cells ANKRD9 localized to vesicles throughout the cytoplasm.

ANKRD9's role as an IMPDH2 partner protein

The second report on the function of ANKRD9 is a proteomics study into the interactome within a cell. Authors mapped the human interactome of HEK293 cells using high throughput affinity purification of 13,000 FLAG-HA tagged open reading frames followed by mass spectrometry (41). They found interacting partners for 2,594 proteins. IMPDH2 (inosine monophosphate dehydrogenase 2), described in Section 1.2, was used as bait and ANKRD9 was found as one its interacting partners. Other proteins found to interact include with IMPDH2 were IMPDH1, PUSL1 (pseudouridylate synthase-like 1), SRP2 (S phase Kinase associated protein) and SMCR8 (Smith-Magenis syndrome chromosome region candidate 8). That ANKRD9 was found as a partner protein for a nucleotide biosynthesis enzyme further shows that ankyrin repeats can take on a variety of important roles.

ANKRD9's role in cell proliferation and interaction with IMPDH2

The third report explores the interaction between ANKRD9 and IMPDH2 in the context of cell proliferation and cancer (42). Authors suggest that ANKRD9 is a part of a ubiquitin-ligase complex that targets IMPDH2 . They describe the subunits of a CUL-5 (cullin-5) ubiquitin ligase (E3) complex which includes a scaffold, adaptor, RING domain binding to E2 and substrate receptor. The authors propose that ANKRD9 serves as the substrate receptor where IMPDH2 is the substrate for ubiquitination and degradation.

To arrive at this conclusion, ANKRD9 was initially identified as a cancer associated gene in this report. Cancer patients and controls were genotyped for 13 ANKRD9 single nucleotide polymorphisms to determine association with susceptibility to gastric cancer;

previous reports showed that ANKRD9's expression was reduced in gastric cancer (43). FLAG-tagged ANKRD9 was then used to show that overexpression of ANKRD9 reduced proliferation of human MKN45 cancer cells while ANKRD9 knockdown increased proliferation.

ANKRD9 was then identified as having a SOCS (suppressor of cytokine signaling) box which is typical of substrate receptor proteins in ubiquitin ligase complexes. It has also been shown that Asb11 (ankyrin repeats and SOCS box 11) is a member of ubiquitin ligase complex (44). SOCS-box containing proteins can bind other subunits of CUL-5 ubiquitin ligase complexes; the authors showed that ANKRD9 binds to ELOB-C and CUL5 with co-transfection of the ANKRD9 SOCS box and ELOB (elongin-B) and ELOC (elongin-C). The authors therefore concluded here that ANKR9D is an ASB (ankyrin repeats and SOCS box, described above).

The authors lastly explored ANKRD9's relationship with IMPDH2 as it was identified from Co-IP mass spectrometry experiments with FLAG-ANKRD9 as bait. They found that ANKRD9 specifically contributes to IMPDH2 degradation through the ubiquitin-ligase complex where ANKRD9 overexpression lowered IMPDH2 levels and its knockdown increased IMPDH2 levels. Additionally, ANKRD9's function in cells depended on IMPDH2; overexpressing IMPDH2 reduced ANKRD9's impact on cell proliferation. These findings show co-dependence of ANKRD9 and IMPDH2 and point to a specific role of ANKRD9 in cancer cell proliferation. The authors did not, however, show the definitive role of ANKRD9, however, only that it is associated with cell proliferation by lowering IMPDH2 protein levels. They suggest that since IMPDH2 is overexpressed in cancer cells, ANKRD9 may serve to keep IMPDH2 levels lower to prevent cancer cell progression, but this was not confirmed.

These reports point to varied functions of ANKRD9 in cell physiology but so far there is no definitive connection between ANKRD9 roles in lipid metabolism, copper metabolism, and nucleotide metabolism . Our studies into the interaction between ANKRD9 and IMPDH2 provide a first look at the spatiotemporal control of ANKRD9 owing to its distinct cellular forms that may contribute to its varied roles.

Section 1.2: Inosine monophosphate dehydrogenases

Section 1.2.1: IMPDH2 and nucleotide metabolism

IMPDH2 is the rate-limiting enzyme for guanine nucleotide biosynthesis

Inosine monophosphate dehydrogenase 2 (IMPDH2) is the rate-limiting enzyme in guanine nucleotide biosynthesis (45,46). It catalyzes the conversion of inosine monophosphate (IMP) to xanthine monophosphate which is then converted to guanine monophosphate by guanosine monophosphate synthase and finally to guanosine triphosphate through nucleoside diphosphate kinases (46,47). This process constitutes the purine de novo pathway for generating guanosine triphosphate, GTP. The salvage pathway uses guanosine, which is converted to guanine by purine nucleoside phosphorylase. Prior to the action of IMPDH2 there are several steps which begin with PRPP, or phosphoribosyl pyrophosphate, which is the precursor to all purine nucleotides (48), see Figure 3.

IMP can be diverted to ATP synthesis in the de novo pathway if it is converted to adenosine monophosphate by adenylosuccinate synthetase and adenylosuccinate lyase (49). The steps that convert PRPP to IMP use the metabolite glutamine (48,50). For pyrimidine biosynthesis carbamoyl phosphate is converted to uridine triphosphate. CTPS1/2 (cytidine triphosphate synthetase) then converts UTP to CTP (51). CTPS2 is an important enzyme in nucleotide biosynthesis with cellular behavior similar to IMPDH2, described in Section 1.2.2. Guanosine triphosphate is used for DNA/RNA synthesis, glycoprotein synthesis and cell signaling, making it a multi-functioning metabolite (46).

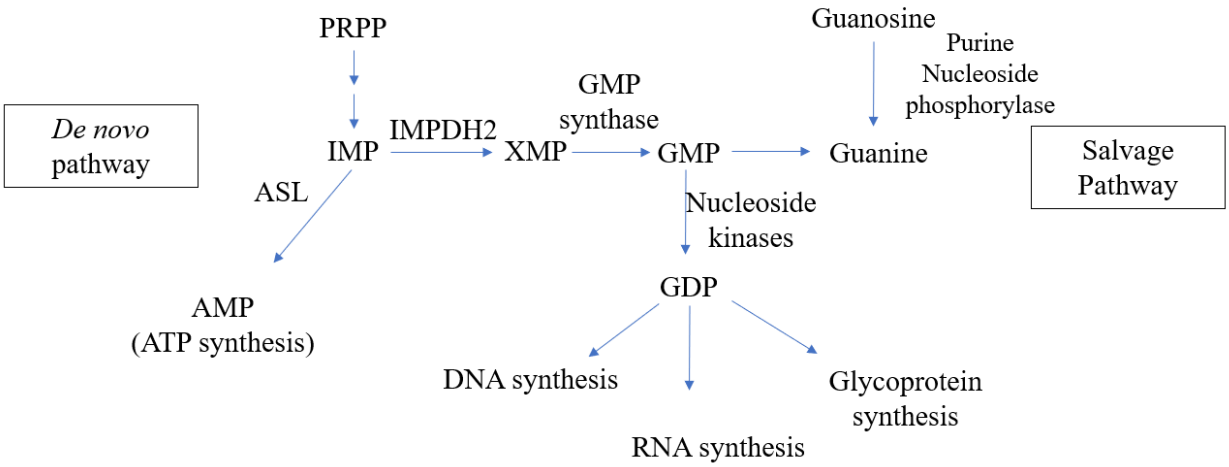

Figure 3: Guanine nucleotide synthesis pathway. The *de novo* pathway (left) uses IMPDH2 to convert IMP to XMP and finally to GDP which is then used for DNA/RNA synthesis as well as glycoprotein synthesis. The salvage pathway (right) uses precursor guanosine to generate GTP. Abbreviations: ASL: adenosylosuccinate lyase, AMP: adenine monophosphate, IMP: inosine monophosphate, PRPP: phosphoribosyl pyrophosphate, IMPDH2: Inosine monophosphate dehydrogenase 2, XMP: xanthine monophosphate, GMP synthase: guanine monophosphate synthase, GDP: guanine diphosphate. Adapted from (46).

Section 1.2.2: Macromolecular assembly

IMPDH2 has a nucleotide-binding regulatory domain

IMPDH2 is a 55 kDa protein with an active site for catalysis and a regulatory domain. Sister enzyme IMPDH1 has 84% sequence identity; IMPDH2 is overexpressed in rapidly proliferating cells (52). The active site contains adjacent substrate (IMP) and cofactor (NAD+, nicotinamide adenine dinucleotide) sites (45-47). The regulatory domain consists of two cystathionine β-synthase (CBS) domains which bind nucleotides to regulate IMPDH2 activity (53,54). In IMPDH2, ATP and GTP bind to activate or inactivate IMPDH2, respectively (54,55). Specifically, ATP stabilizes the IMPDH2 homotetratmer in an open conformation whereas GTP stabilizes the IMPDH2 homotetratmer in a closed conformation (56,57).

In vitro and cellular rod formation

An interesting phenomenon that occurs with IMPDH2 in cells is the formation of rods and rings (RR), also termed cytoophidia, meaning 'snakes' (48,58-62). This occurs under two circumstances, in vitro and in cells without much consensus in the field on whether the structures formed under either of these circumstances are related. The addition of ATP to purified IMPDH2 yields fibrils around 200 nanometers in length, which can be visualized using electron microscopy (63). These are known as higher order oligomers of IMPDH2 tetramers, and whether or not these are active has been an open subject. Some studies report that purified IMPDH2 rods are active as they are formed with ATP and show increases in activity (62). Other studies report that activity is unchanged regardless of ATP addition (63).

In cells, IMPDH2 forms rods and rings that are 3-5 microns long under a variety of circumstances. Amino acid starvation, T cell activation, and inhibition using Ribavirin, Mycophenolic Acid and DHFR (dihydrofolate reductase) inhibitors have been reported as triggers of IMPDH2 rod formation in cells; IMPDH rods also occur naturally in some stem cell lines (48,60,64-66). Mycophenolic acid has been reported to lower IMPDH2 activity and it is proposed that inhibitors lower GTP pools (62,67). Recently rods and rings have been reported in mouse tissue following administration of Ribavirin, a substrate inhibitor used as an antiviral (68). Rod formation is conserved throughout evolution, with rods seen in *Drosophila, S.pombe, S.cerevisea* and human cell lines (66,69,70). They have been shown to form perinuclearly and over time, with time-lapse microscopy showing an increase in rod length over 2 hours after Mycophenolic Acid treatment (64).

Rod reversal and the importance of guanosine

So far, the only known metabolite that reverses rod formation in cells is the addition of guanosine; conversion to guanine occurs with purine nucleoside phosphorylase found in FBS (fetal bovine serum) in complete medium (67). Explanations for guanosine-mediated disassembly of IMPDH2 rods include having an excess of this final product.(62,67). That Ribavirin, substrate inhibitor of IMPDH2 and rod formation trigger, has its effect reversed by guanosine supports this idea. However, the fact that GTP binds to the regulatory domain of IMPDH2 and forces a closed inactive conformation has not been reconciled with the observation that guanosine reverses rod formation; it is possible that reversal of IMPDH2 rods with guanosine is due instead to GTP directly binding IMPDH2.

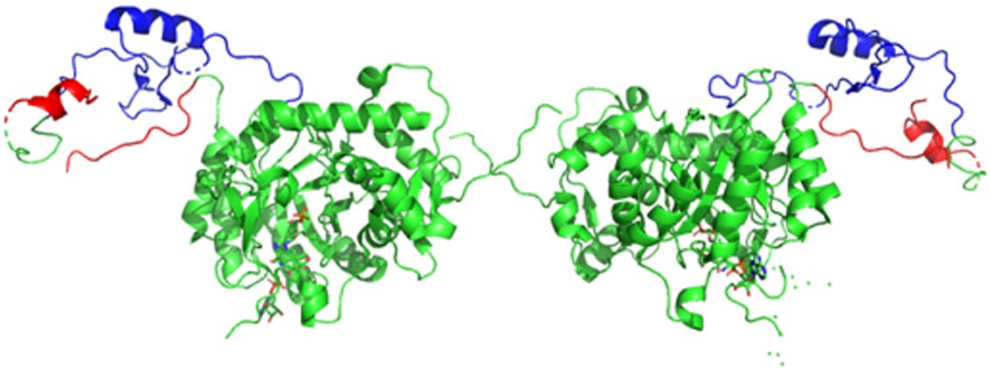

Figure 4: IMPDH2 dimer, PDB 1NF7. In red and blue are CBS domains 1 and 2 which bind nucleotides. CTPS2 binds nucleotides but does not contain CBS domains, which in Chapter 2 of this dissertation interact with ANKRD9.

Rod formation also occurs with related enzyme CTPS2 but responds differently to nucleotides

Rod formation has been reported for other metabolic enzymes including CTPS2, which forms rods following inhibition by DON (6-diazo-5-oxo-L-norleucine) (59,71). It has been shown that formation of rods by human CTPS2 enhances catalytic activity whereas bacterial CTPS2 rod formation lowers activity, further compounding the rod formation phenomenon (72,73). Two reports investigated IMPDH2/CTPS2 rod formation together. The first concluded that IMPDH2 and CTPS2 rods were generally separated. DON specifically converts CTPS2 into rods without affecting IMPDH2, whereas Ribavirin triggers appearance of both IMPDH2 and CTPS2 rods (61). The second report concluded that IMPDH2 and CTPS2 have interfilament interactions (74). Of note, CTPS2 rods are generally longer than IMPDH2 rods (70).

Nucleotide binding consequences are different for the enzymes. It has been found that while GTP inhibits IMPDH2 and disassembles rods, it enhances CTPS2 activity, perhaps to balance purine and pyrimidine synthesis (72). In addition, ATP, UTP and CTP have been shown to influence tetramerization of CTPS2, whereas IMPDH2 oligomerizes with ATP addition and disassembles with GTP addition (note that this oligomerization is with purified CTPS2 and IMPDH2) (73). Also while IMPDH2 has canonical CBS domains described above (and shown in Figure 4) for nucleotide binding, CTPS2 does not have CBS domains but does have putative nucleotide binding sites, as reported for *E.coli* CTP synthase and human CTP synthase (72,73).

Thus, while both IMPDH2 and CTPS2 can form rods, IMPDH2 has specific requirements for doing so where CTPS2 has many more factors that influence its oligomerization. CTPS2 can assemble and disassemble in response to a variety of metabolites but IMPDH2 can only do so with the ATP/GTP pair, primarily owing to the canonical CBS domains which are not present in CTPS2. These differences in CTPS2 and IMPDH2 responses to regulator molecules provides further evidence for the specificity of the ANKRD9-IMPDH2 interaction that we observed in our work (see Chapter 2).

Why rods are formed is an open question

Explanations for rod formation include: a storage depot, to enhance or inhibit catalytic activity, and as simple aggregates without specific function (66,70,75). For example, one model posits that CTPS2 forms oligomeric rods that are inactive whereas the homotetramer is active (70). Recently another enzyme -asparagine synthetase- has been reported to form rods with AICAR (5-aminoimidazole-4-carboxamide ribonucleotide), an analog of AMP that stimulates AMPK activity (76). While more enzymes have been added to the growing list of proteins capable of forming rods, protein lacking enzymatic activity have not been reported to form rods. Our studies provide a first such example in the case of ANKRD9 and investigate functional significance.

Section 1.2.3: IMPDH2 and ANKRD9

ANKRD9 was identified as part of a ubiquitin ligase complex where IMPDH2 was the substrate for degradation (described in Section 1.1.4) (41,42). While this report was the first to describe the potential role of the ANKRD9-IMPDH2 interaction (a prior proteomics screen identified IMPDH2 and ANKRD9 as partner proteins) we address how ANKRD9 could regulate IMPDH2 abundance and macroassembly.

Our studies show that ANKRD9 indeed forms rods which co-localize with IMPDH2 rods in response to nutrient deprivation and IMPDH2 inhibition with Ribavirin. We also show that guanosine reverses ANKRD9/IMPDH2 rods and identify residues for ANKRD9 rod formation and ANKRD9/IMPDH2 interaction. This work supports the idea that ANKRD9 stabilizes IMPDH2 under certain metabolic conditions in the form of rods. Importantly, rod formation could be used to protect IMPDH2 from ANKRD9-dependent degradation, which may occur through the CUL-5 ubiquitin ligase described in the previous report. Another model supporting this theory is that IMPDH2 rods are inactive to keep from degradation (66). Also of note is the observation that rod formation does not occur with IMPDH2 CBS domain deletion (54), which fits with our data as ANKRD9 and IMPDH2 interact within the CBS domains in the vicinity of the IMPDH2 nucleotide binding site (see Figure 12 in Chapter 2, Section 3.2). This work shows that an ankyrin-domain containing protein is capable of forming rods under specific metabolic conditions where rod reversal is controlled by similar factors that regulate the nucleotide biosynthesis enzyme IMPDH2.

Chapter 2: ANKRD9 is a metabolically-controlled regulator of IMPDH2 abundance and macro-assembly

Modified from: Hayward et. al. ANKRD9 is a metabolically-controlled regulator of IMPDH2 abundance and macro-assembly. *Submitted.*

Chapter 2: ANKRD9 is a metabolically-controlled regulator of IMPDH2 abundance and assembly

Section 2.1: Introduction

Ankyrin Repeat Domain proteins (ANKRD) form a large and fascinating family of proteins that regulate numerous cellular proteins and pathways. The activities of ANKRDs involve protein complex assembly, interactions with the cytoskeleton, post-translational modifications, regulation of protein degradation and many others (3,5,7,9,11,13,25,27). Structural basis of interactions between ANKRDs and their targets is becoming clearer (3), however little is known about regulation of these interactions in cells. In some cases, the same ANKRD binds to different protein targets and modulates distinct cellular pathways, these different forms of action remain poorly understood.

ANKRD9 (ankyrin-domain containing protein 9) is an ankyrin-domain containing protein implicated in a broad spectrum of cellular processes, including lipid metabolism (40), copper homeostasis (37) and cell proliferation (42). Recent genome-wide association studies have uncovered the potential role of ANKRD9 in hypertension (77) and myocardial repolarization(78). Despite the accumulating evidence of ANKRD9's physiologic and clinical significance, information about functional properties and mechanisms of ANKRD9 are very limited. Analysis of the protein sequence predicted ANKRD9 to be a 35 kDa protein with at least one ankyrin repeat. In a large mass-spectrometry screen of the human interactome, ANKRD9 was co-purified with inosine monophosphoate dehydrogenase 2 (IMPDH2) (41), the rate limiting enzyme in GTP biosynthetic pathway. Recent studies confirmed this interaction and found that overexpression of ANKRD9 decreases IMPDH2

levels by stimulating interactions with the ubiquitin-ligase complex and causing protein degradation (42).

These findings are difficult to reconcile with the original report, which demonstrated that in cells ANKRD9 was targeted to vesicle-like structures (40) and could therefore be spatially separated from IMPDH2, which is a cystolic enzyme. ANKRD9 mRNA levels are under nutritional control (40) and therefore it is possible that the ANKRD9 protein has different localization and functions under different metabolic conditions. Our studies have tested this hypothesis. We have found that the intracellular location of ANKRD9 and its regulation of IMPDH2 depend on availability of metabolites (guanosine) as well as a tertiary structure of IMPDH2. Taken together, our results suggest a mechanism through which ANKRD9 modulates the intracellular properties of IMPDH2 in response to metabolic changes.

Section 2.2: Results

In cells, ANKRD9 adopts two distinct forms.

This work started with an observation that expression of a FLAG-tagged ANKRD9 in HeLa cells produced two very different intracellular patterns. In the majority of cells, ANKRD9 was associated with vesicles (Fig. 4a), in agreement with a previous report (40), whereas in some cells ANKRD9 was present in distinct 3-5 microns "rod-like" structures (Fig. 5a, arrows). While vesicles were numerous and distributed throughout the cell, typically only few (1-3 per cell) rods were formed in the cytoplasm and around the nucleus. The appearance of the rods was intriguing, because IMPDH2 (an established target of ANKRD9) is known to assemble into rod-like filaments (also called cytoophidia) in response to various metabolic perturbations (48,58-60,62,65,79).

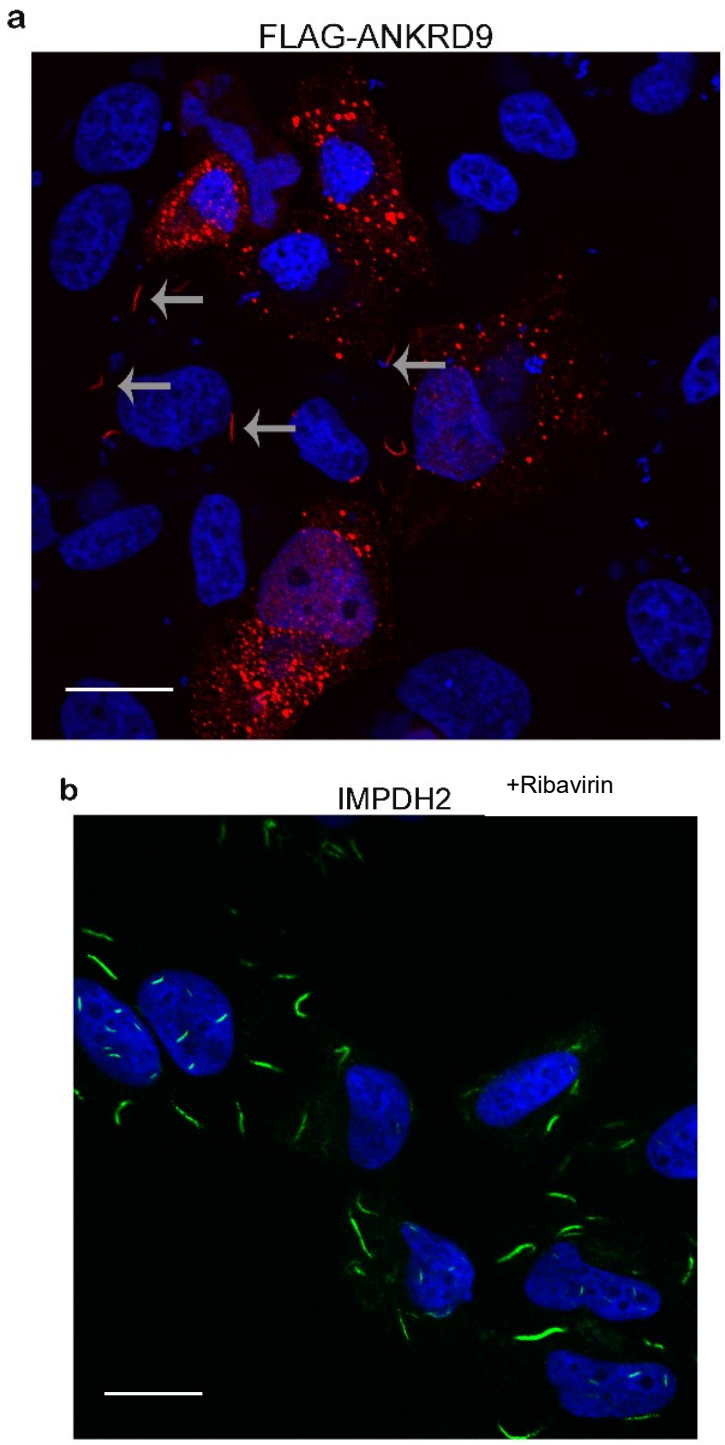
a
FLAG-ANKRD9
b
IMPDH2
+Ribavirin

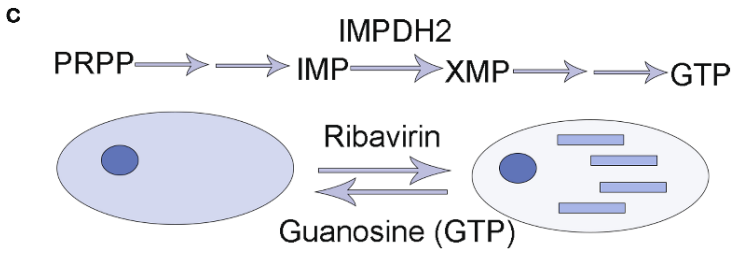
c
IMPDH2
PRPP
IMP
XMP
GTP
Ribavirin
Guanosine (GTP)

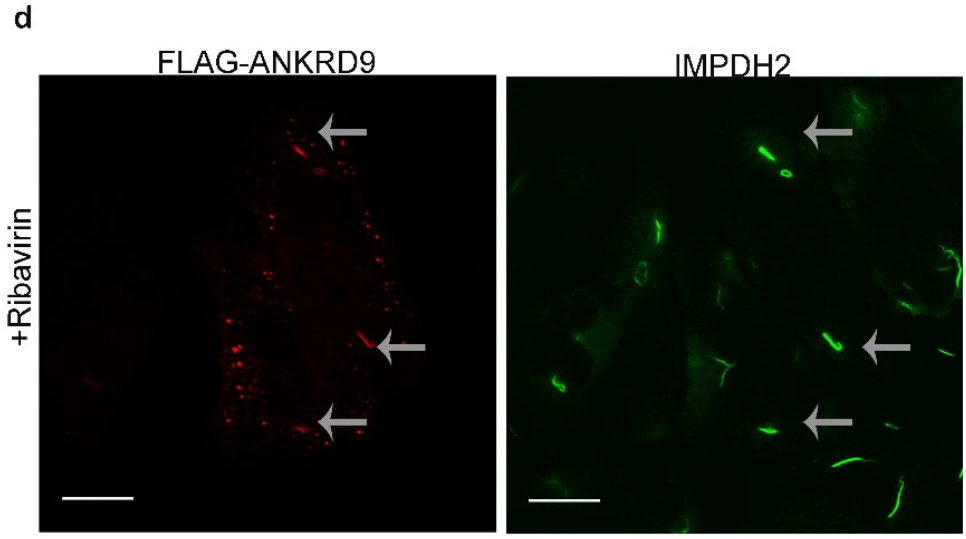
d
FLAG-ANKRD9
IMPDH2
+Ribavirin

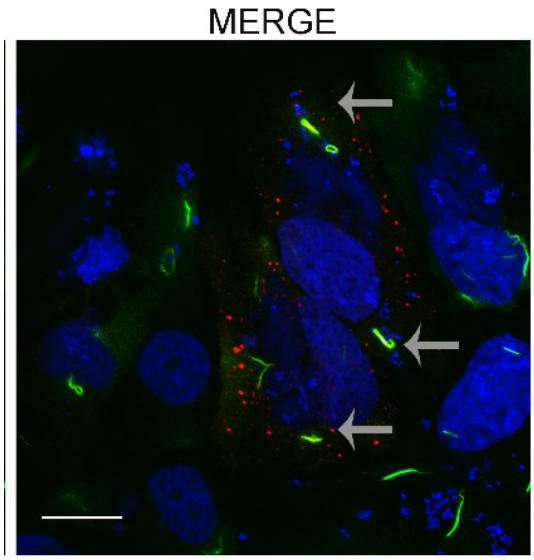
MERGE

Figure 5: ANKRD9 adopts two distinct forms (a) HeLa cells were transfected with FLAG-ANKRD9 expressing plasmid and immuno-stained for the FLAG-tag. FLAG-ANKRD9 (red) shows a vesicular and rod-like pattern (gray arrows); cell nuclei are visualized with DAPI (blue); n=3. (b) Inosine monophosphate dehydrogenase 2 (IMPDH2) forms rods when inhibited with Ribavirin. HeLa cells were treated with 10 μM Ribavirin for 1hr then stained for IMPDH2 green) and DAPI (blue); n=2. (c) IMPDH2 mediates the rate limiting step (conversion of inosine monophosphate, IMP, to xanthine monophosphate, XMP) in a pathway beginning with phosphoribosyl pyrophosphate (PRPP) and eventually leading to guanosine triphosphate, GTP. IMPDH2 transitions from a diffuse cytosolic form (left) to rods (right) when inhibited with Ribavirin; this transition is reversed with guanosine. (d) HeLa cells were treated with 10 μM Ribavirin for 1 hour then transfected with FLAG-ANKRD9 for 16hrs and immuno-stained for FLAG (green) and IMPDH2 (red). Gray arrows point to rods containing both IMPDH2 and ANKRD9. Scale bar: 20 μm.

Formation of IMPDH2 rods can be rapidly induced by incubating cells with Ribavirin, a potent cell-permeable inhibitor of IMPDH2 (Fig. 5b,c). Consequently, to test whether the recombinant ANKRD9 associates with IMPDH2 in rods, we treated cells with Ribavirin for 1 h prior to ANKRD9 expression. Under these conditions, ANKRD9 co-localized with the IMPDH2 rods and was also detected in vesicles in the same cells (Fig. 5d). The overlap between ANKRD9 and IMPDH2 in rods was complete, i.e. no ANKRD9-rods without IMPDH2 was detected. Thus, in addition to the "basal" vesicular form, ANKRD9 interacts with the inactive IMPDH2 in rod-like filaments.

ANKRD9 forms rods upon nutrient limitation

These results were interesting because they demonstrated the previously unknown ability of ANKRD9 to assemble with IMPDH2 in large macromolecular complexes. To better understand the physiologic basis of ANKRD9/IMPDH2 assembly we considered that ANKRD9 mRNA levels respond to starving/re-feeding (i.e. are nutrient dependent (40)) and that IMPDH2 forms rods when cells are starved of certain metabolites (48,65). Consequently, we tested whether nutrient deprivation would cause transition of ANKRD9 from vesicles to rods. Cells transfected with ANKRD9 plasmid were grown in low serum (0.1% FBS) for 24 and 48 hours and stained for ANKRD9 and IMPDH2. After 48 hours of nutrient limitation *all* ANKRD9 was found in rods (compare Fig 6a and 6b). The transition from vesicles to rods was time dependent (Fig. 6c); i.e. after a shorter nutrient limitation - 24 hours – ANKRD9 was detected in both vesicles and rods (Fig. 6c,d).

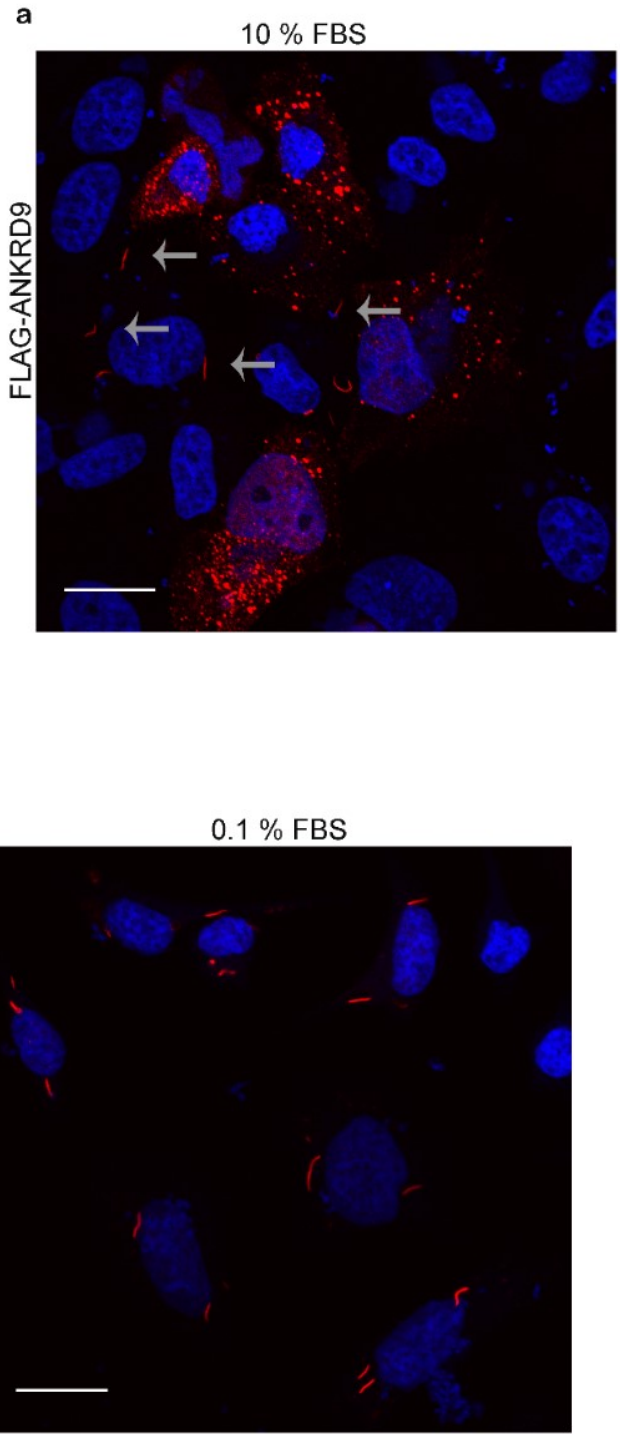
a
10 % FBS
FLAG-ANKRD9
b
0.1 % FBS

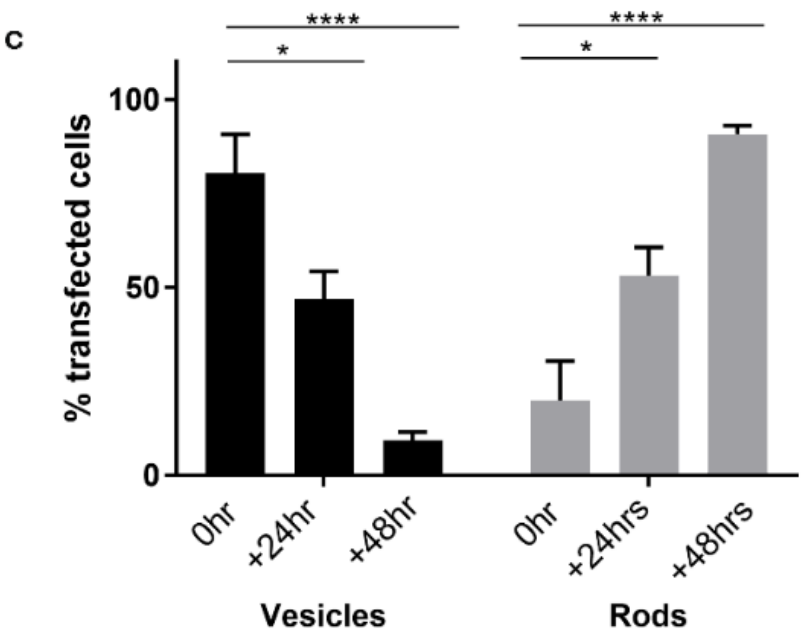
c
****
*
****
*
100
50
0
% transfected cells
0hr
+24hr
+48hr
0hr
+24hrs
+48hrs
Vesicles
Rods

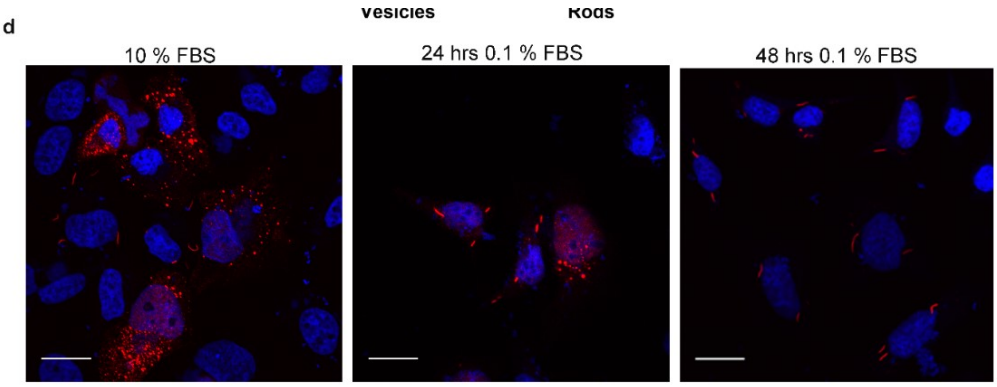
d
Vesicles
Rods
10 % FBS
24 hrs 0.1 % FBS
48 hrs 0.1 % FBS

Figure 6: ANKRD9 forms rods upon nutrient depletion. HeLa cells were transfected with FLAG-ANKRD9 (red) as in Fig 5a and incubated in the presence of 10%FBS (a) or 0.1% FBS (b) for 48 hrs. Rods are indicated by gray arrows; nuclei are stained with DAPI (blue); n=3 (c) Percentage of cells containing ANKRD9 in vesicles (black) or rods (grey) after overnight transfection (control), followed by 24 hrs or 48 hours in starvation (0.1% FBS) media. Total number of analyzed cells: n=137 (control); 149 (24h), and 131 (48h); Error bars represent standard error. Two-way ANOVA was used to determine p-values (*, p value = 0.03, ****, p value < 0.0001) (d) Representative images of each timepoints; rods appear in the majority of cells after 48 hours in 0.1 % FBS media. Scale bar: 20 μm.

Formation of ANKRD9 rods is caused by depletion of IMPDH2 dependent metabolites.

Brief treatment of cells with Ribavirin and a prolonged nutrient depletion both cause IMPDH2 inhibition and the ANKRD9/IMPDH2 assembly. In the first case, the vesicle-to-rod transition of ANKRD9 was partial, whereas in the second case it was complete. One important difference between these two conditions is the duration of IMPDH2 inactivation. Partial effect of brief treatment with Ribavirin suggested that the inhibition of IMPDH2 *per se* could be insufficient for ANKRD9 dissociation from vesicles and that the depletion of IMPDH2-dependent metabolite(s) may be needed for complete conversion of ANKRD9 into a rod-bound form. To test this hypothesis, we added Ribavirin to cells prior to ANKRD9 expression, as previously, and then allowed cells to grow for 24 and 48 hours under basal conditions (i.e. in normal serum) in the presence of Ribavirin (Fig. 7).

After 24 hours, ANRKD9 fully transitioned to rods (Fig. 7b). The rods contained both ANKRD9 and IMPDH2 and were very similar to those induced by 48 hours of nutrient limitation (compare Fig. 7a and Fig. 7b). The result suggests that the prolonged incubation with the IMPDH2 inhibitor mimics serum starvation conditions, i.e. the treatment depletes cells from IMPDH2-dependent metabolites.

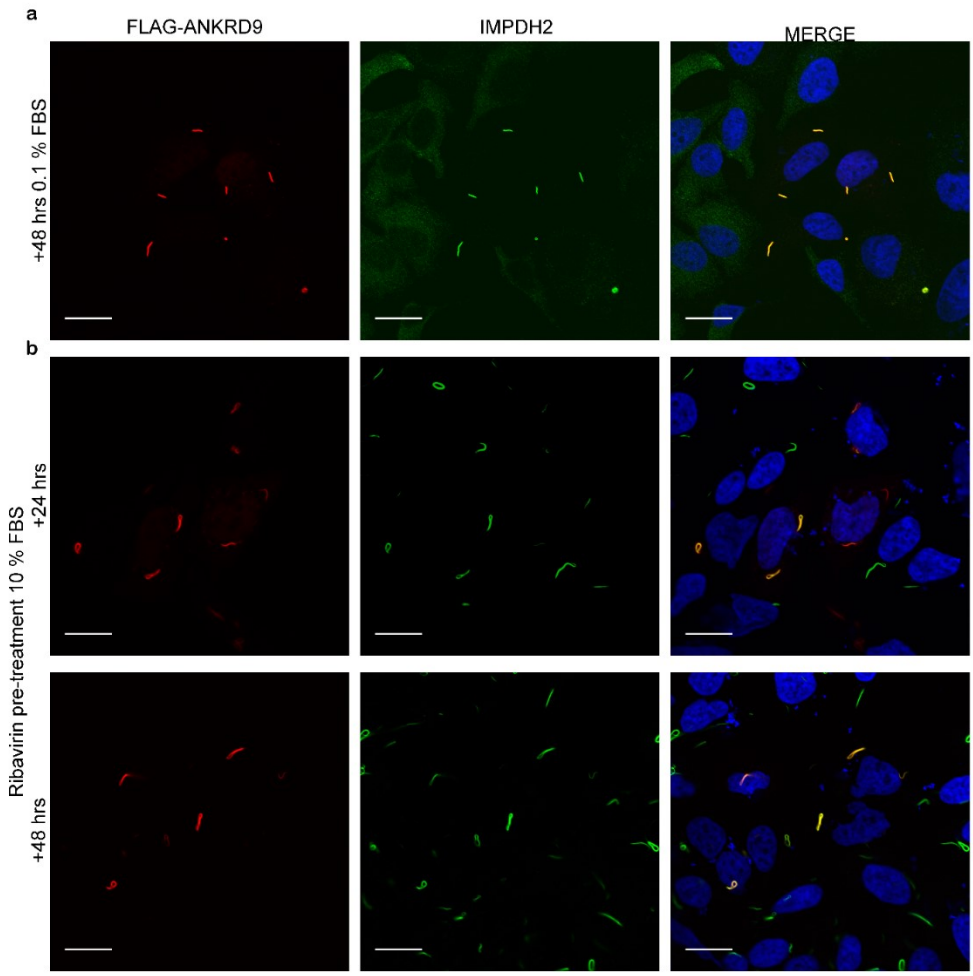

Figure 7: Formation of ANKRD9 rods is caused by depletion of IMPDH2 metabolites (a) HeLa cells were transfected with FLAG-ANKRD9 then placed in 0.1% FBS for 48 hours and immunostained for FLAG and IMPDH2; n = 3 (b) HeLa cells were treated with 10 μM Ribavirin for 1 hour then transfected with FLAG-ANKRD9 and kept in 10% FBS for 24 and 48 hours. Cells were immunostained with anti-FLAG (red) and anti-IMPDH2 (green) antibodies; n=2. Merged images show complete overlap between ANKRD9 and IMPDH2 rods. Scale bar: 20 μm.

Guanosine reverses the ANKRD9 relocalization from vesicles to rods

To test further whether the vesicle-to-rod transition of ANKRD9 represents a regulatory response to metabolic state of the cell, we tested whether the ANKRD9 transition to rods can be reversed. First, cells were grown under nutrient limiting conditions for 24 hours to induce rod formation, then washed and placed into the basal growth medium for 24 hours. This treatment decreased the abundance of rods and caused appearance of vesicles, but did not fully restore ANKRD9 targeting to vesicles (Fig 8). We then considered that the depletion of guanine pools was previously suggested to cause IMPDH2 macro-assembly and that IMPDH2 rods can be disassembled by guanosine addition (62,67).

Consequently, we tested whether the ANKRD9/IMPDH2 rods, formed under conditions of nutrient limitation, were affected by guanosine. To this end, we expressed FLAG-ANKRD9, induced rod formation by incubating cells for 48 hrs in low serum and then added 100 μM guanosine for 1hr (this concentration was previously shown to reverse IMPDH2 rod formation (Fig. 9, (67)). Addition of guanosine completely reversed the ANKRD9 assembly with IMPDH2 and caused uniform transition of ANKRD9 back to vesicles (compare Fig. 9a and 9b). This effect was rapid; the vesicular pattern of ANKRD9 was already observed at 10 minutes following addition of guanosine (Fig. 9c). Thus, the disassembly of ANKRD9 occurs on a much faster timescale than rod formation, perhaps reflecting addition of a large excess of guanosine. Guanosine-dependent change in ANKRD9 pattern also suggests that cellular behavior of ANKRD9 may be controlled by the same factors that regulate IMPDH2 macroasssembly, specifically, lower guanine pools.

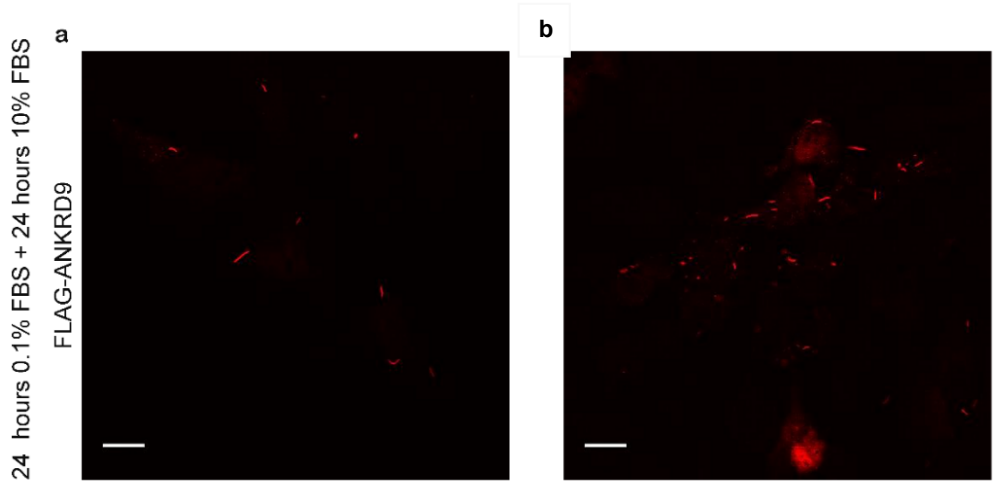

Figure 8: Serum re-addition partially reverses rod formation in ANKRD9. HeLa cells were transfected with FLAG-tagged ANKRD9 and incubated under nutrient limiting conditions (0.1% FBS) for 24 hours, then cell growth medium was replaced with the medium containing 10% FBS. Cells were incubated for another 24 hours and then immunostained for FLAG. Both (a) and (b) are representative images of cells after the above conditions. The 24 hours nutrient limitation induces ANKRD9 transition from vesicles to rods in approximately 50% of cells (see Figure 6). Placing cells in 10% serum for 24 hours only partially reverses this phenotype i.e some cells still have ANKRD9 in rods (long and short) and other cells show mostly punctate/vesicular pattern, n=2 Scale bar: 20 microns.

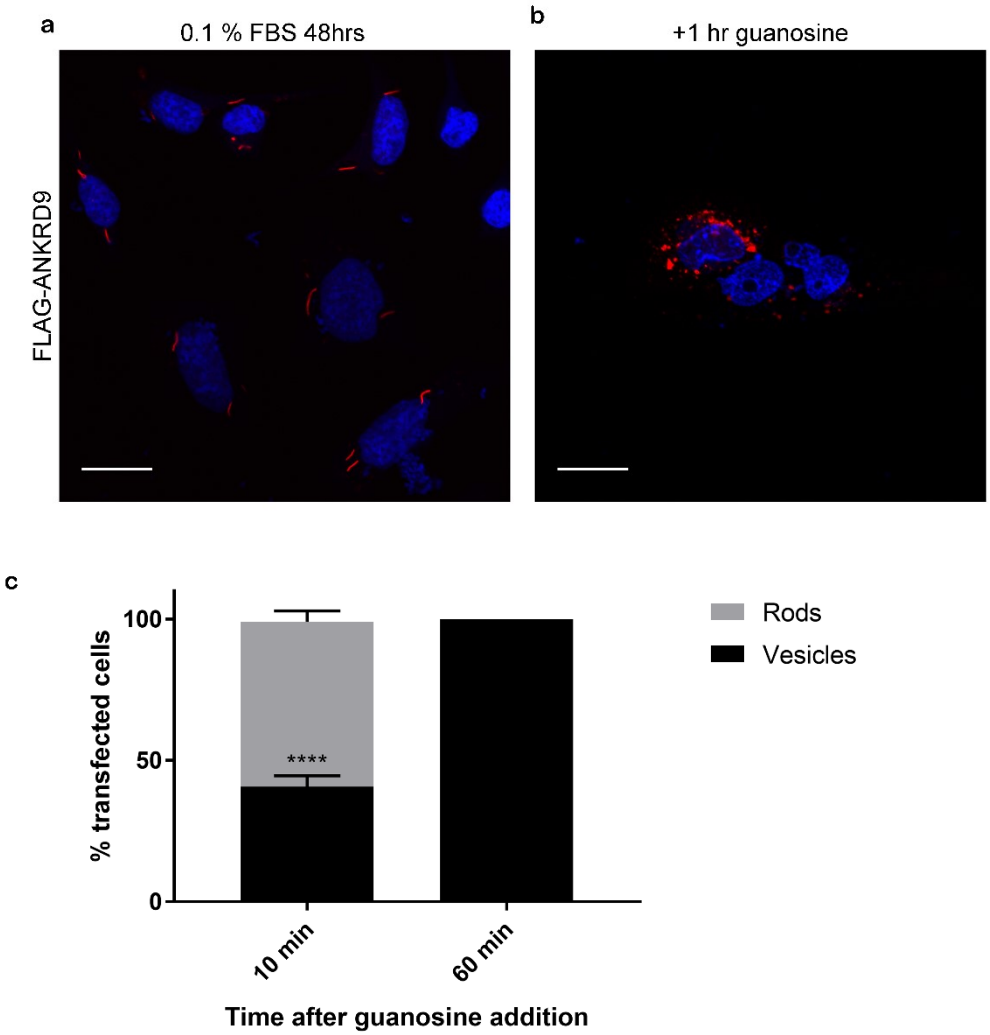

Figure 9: ANKRD9 transition to rods is reversible with guanosine addition (a) Control: FLAG-ANKRD9 forms rods following incubation of HeLa cells in 0.1% FBS for 48hrs; (b) The same treatment, followed by incubation with 100 μM guanosine for 1hr. The ANKRD9 rods disappear and ANKRD9 shows a vesicular pattern; (c) Percentage of cells with ANKRD9 vesicles or rods at 10 and 60 min following addition of guanosine. The number of ANKRD9 rods at 10 and 60 min was compared using unpaired t test. n=3 for each time point; Error bars represent SEM. ****, p value <0.0001. Scale bar: 20 μm.

ANKRD9 expression is associated with longer and fewer IMPDH2 rods

Purified IMPDH2 can assemble into rods *in vitro* in the absence of any other proteins (54,55,63,66,70,80). Therefore, the role of ANKRD9 in IMPDH2 rods is likely to be regulatory and involve modulation of rods' properties. It was previously shown that IMPDH2 rods were dynamic and could change their length over time. Consequently, to clarify the functional significance of ANKRD9/IMPDH2 macro-assembly, we compared the length and numbers of IMPDH2 rods in cell with endogenous and overexpressed ANKRD9 under conditions of nutrient limitation. Ribavirin treatment was used as a control for rod formation. In nutrient-depleted HeLa cells (that have endogenous ANKRD9), the length of IMPDH2 rods was about 1.5 microns, whereas in HeLa cells overexpressing FLAG-ANKRD9 the length of IMPDH2 rods was significantly increased to 3-5 microns (Fig. 10a,b). Note that ANKRD9 endogenous levels in HeLa cells are very low, HEK293A cells were used in knockdown experiments to determine ANKRD9's role.

The length of IMPDH2/ANKRD9 rods is similar to IMPDH2 rods formed in the presence of Ribavirin (Fig 10c). This result further suggests that under conditions of nutrient limitation ANRKD9 binds to an inhibited IMPDH2. An increased length of IMPDH2 rods suggested that excess ANKRD9 stabilizes the IMPDH2 rods favoring longer structures. Indeed, we found that without ANKRD9 overexpression the number of IMPDH2 rods per cell was about 6, whereas significant increase in rods length upon ANKRD9 overexpression was associated with the decreased number of rods - to about 2 per cell (Fig 10d).

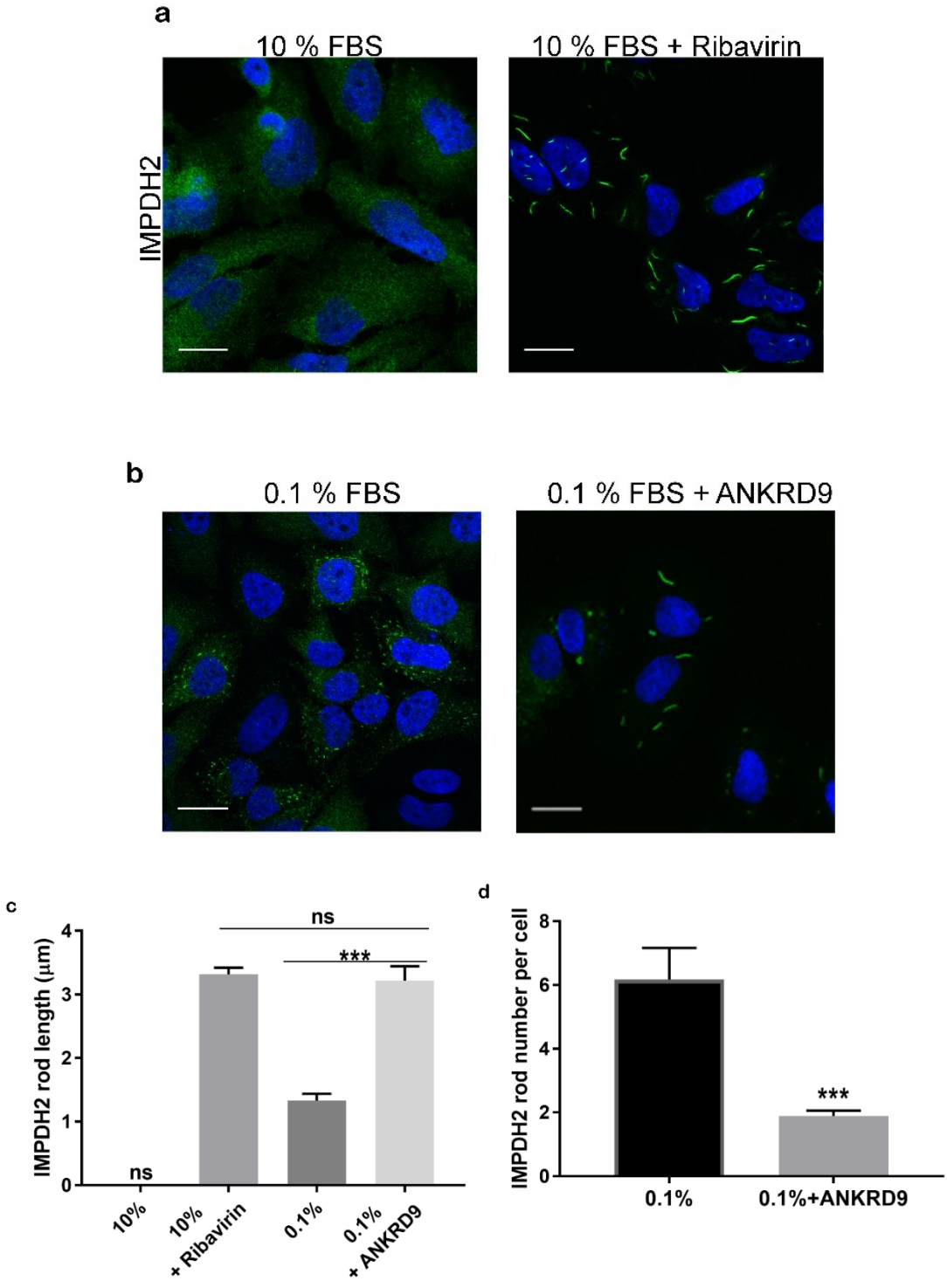
a
10 % FBS
10 % FBS + Ribavirin
IMPDH2
b
0.1 % FBS
0.1 % FBS + ANKRD9
c
IMPDH2 rod length (μm)
ns
***
ns
10%
10% + Ribavirin
0.1%
0.1% + ANKRD9
d
IMPDH2 rod number per cell
***
0.1%
0.1%+ANKRD9

Figure 10: *Higher ANRKD9 abundance is associated with longer IMPDH2 rods*. *(a) Control: immunostaining of IMPDH2 in HeLa cells under basal conditions shows an expected diffuse pattern (left panel). Treatment of these cells with 10 μM Ribavirin for 1 hour in the absence of recombinant ANKRD9 triggers formation of IMPDH2 rods (right panel). (b) Left panel: In the absence of recombinant ANKRD9, nutrient limitation (0.1 % FBS for 48 hours) causes appearance of short IMPDH2 rods. Right panel: Expression of recombinant FLAG-ANKRD9 significantly increases the length of IMPDH2 rods (c) Quantitation of IMPDH2 rod length in different treatment conditions (d) Quantitation of number per cell under nutrient limitation in the absence and presence of recombinant ANKRD9. Excess ANKRD9 favors formation of longer and fewer IMPDH2 rods. Number of cells: treatment with Ribavirin (n = 150), nutrient limitation (n =73) of non-transfected cells. For nutrient limitation with FLAG-ANKRD9 expression, n = 156. Statistical analysis of data was done using an unpaired t test, ****, p , 0.001. Error bars represent standard error. Scale bar: 20 microns.*

A conserved CysCys motif is required for ANKRD9 vesicle-to-rod transition

ANKRD9 has not been characterized biochemically and its structure is unknown. Consequently, to better understand the biochemical basis of ANKRD9/IMPDH2 interactions, we predicted the structure of ANKRD9 using the Robetta server (Fig. 11a). The molecular model of ANKRD9 shows nine helix-turn-helix repeats assembled into a concaved structure. To identify amino-acid residues important for ANKRD9 function, we searched for highly conserved residues that are located at protein surface and therefore available for protein-protein interaction. ANKRD9 is highly conserved, but the sequence alignment of ANKRD9 orthologs from multiple species identified several invariant residues in the loop regions of ANKRD9 (Fig. 11a). Two conserved vicinal cysteines $Cys^{109}Cys^{110}$ (Fig. 11b) were of particular interest, because cysteines are susceptible to various modifications and hence can contribute to observed changes in ANKRD9 intracellular behavior.

To directly test the role of $Cys^{109}Cys^{110}$ motif in rod formation we generated a series of mutants, in which Cys^{109} and Cys^{110} were converted to serine individually or together. The C109S, C110S and C109S/C110S mutants were expressed in HeLa cells and their ability to form rods was analyzed under nutrient-limiting conditions. Unlike WT ANKRD9, which shows complete transition to rods after 48 hrs in 0.1% FBS, none of the mutants lost association with vesicles and formed rods under these conditions (Figure 11c). This result suggests that while Cys109 and Cys110 do not play an important role in ANKRD9 binding to vesicles, they are required for rod formation under nutrient limitation.

a

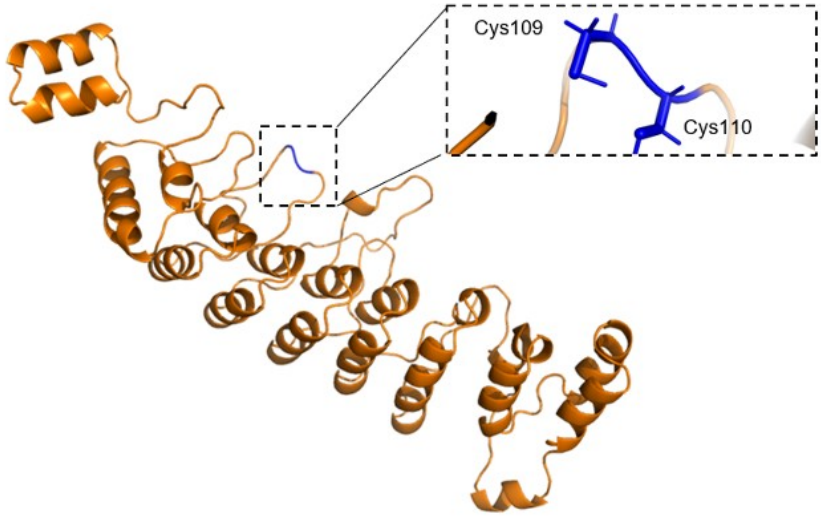

b

CysCys motif conservation

H.sapiens	83	DHQAYAHYLLATFPRRALAPPSAGFRCCAAP-GPHVALA	121
B.taurus	83	DHQGYAHYLLATFPRRALAPPSAGFRCCAAP-GPHVALA	121
R.norvegicus	82	DHQAYAHYLLATFPRRALAPPSAGFRCCTAP-GPHVALA	120
P.lepturus	56	DHQPYAQHLLTKFPQSALAVPSQSFSCCQSS-APHLAMA	94
D.rerio	73	DHQQYARYLLKLFSSRALEMPSRSFCCCQASTAPHLSIA	111
A.calliptera	73	DHQDYAQYLLNRYSVSALRAPRCSYCCCRGSGAPHLNIA	111
P.bivittatus	48	NHLR-VQYLLFQFPEEALKVAGEHFWCCP-SSDSHLAMA	86

c

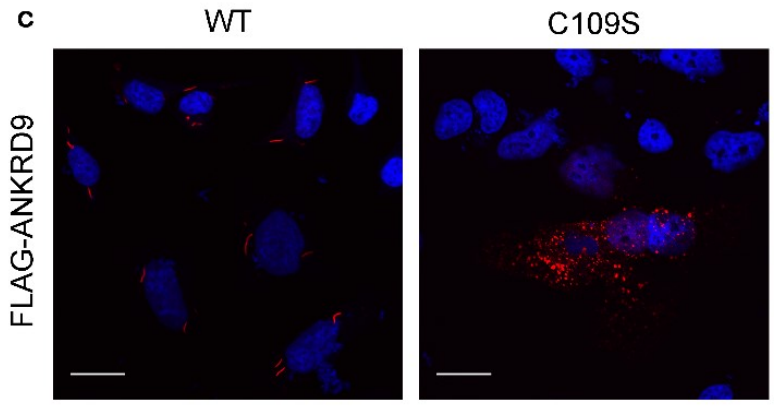

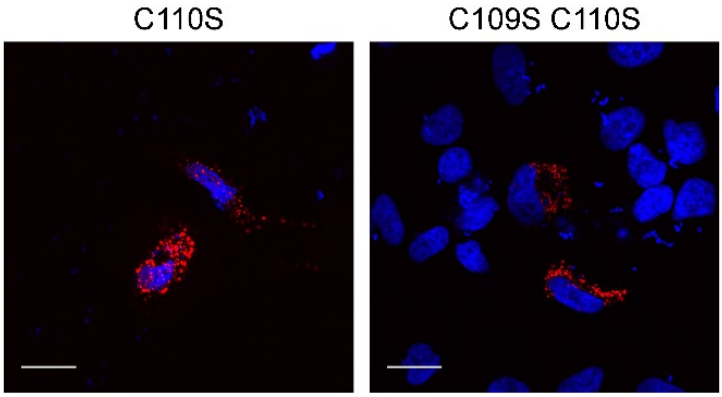

Figure 11: A conserved CysCys motif in ANKRD9 is required for vesicle to rod transition (a) Structural model of the entire ANKRD9 protein with conserved Cys residues highlighted in blue; the boxed area shows the position of Cys109 and Cys110 in the loop (b) Multiple sequence alignment of the CysCys-containing region illustrates conservation of this motif. (c) HeLa cells transfected with WT ANKRD9 (control) or indicated ANKRD9 mutants were placed in 0.1% FBS-containing medium for 48 hours. Unlike WT, none of the mutants formed rods under these conditions. Scale bar: 20 μm.

CysCys motif contributes to ANKRD9-IMPDH2 interaction

The observed inability of $Cys^{109}Cys^{110}$ mutants to leave vesicles and form rods may reflect the role of this motif in "sensing" the metabolite depletion. To determine whether the Cys residues were involved in binding and regulation of IMPDH2, we first explored the possible structural interactions between ANKRD9 and IMPDH2 by docking our Robetta model and the known crystal structure of IMPDH2 (Figure 12a, left panel). The docking revealed favorable interactions between the ANKRD9 loop containing the $Cys^{109}Cys^{110}$ motif with the regulatory domain of IMPDH2 (Fig. 12a, right panel), near the reported nucleotide binding site of IMPDH2 (Fig 13 (54)).

To directly verify these interactions and their consequences, we took advantage of the report that appeared when this work was on-going (42). The published study suggested a role for elevated ANKRD9 in proteasome-mediated degradation of IMPDH2. Consequently, we expressed the WT ANKRD9 and ANKRD9 mutants in HeLa cells under basal conditions and compared their effect on IMPDH2 abundance. Although the intracellular localization of WT and mutants, in vesicles, was very similar, their effects on IMPDH2 levels were drastically different.

Expression of WT ANKRD9 was associated with a marked decrease in staining of IMPDH2 protein, as evidenced by confocal imaging (Fig. 12b). This effect was specific for IMPDH2, as overexpression of ANKRD9 did not influence levels of CTP synthase 2, CTPS2 (Fig. 14a,(71-73,81,82)), another metabolic enzyme known to form rod-like structures. Use of proteasome inhibitor MG132 after transfection with WT ANKRD9 prevented decrease of IMPDH2 levels (Fig. 14b) supporting the proposed role for ANKRD9 in facilitating proteasomal degradation of IMPDH2.

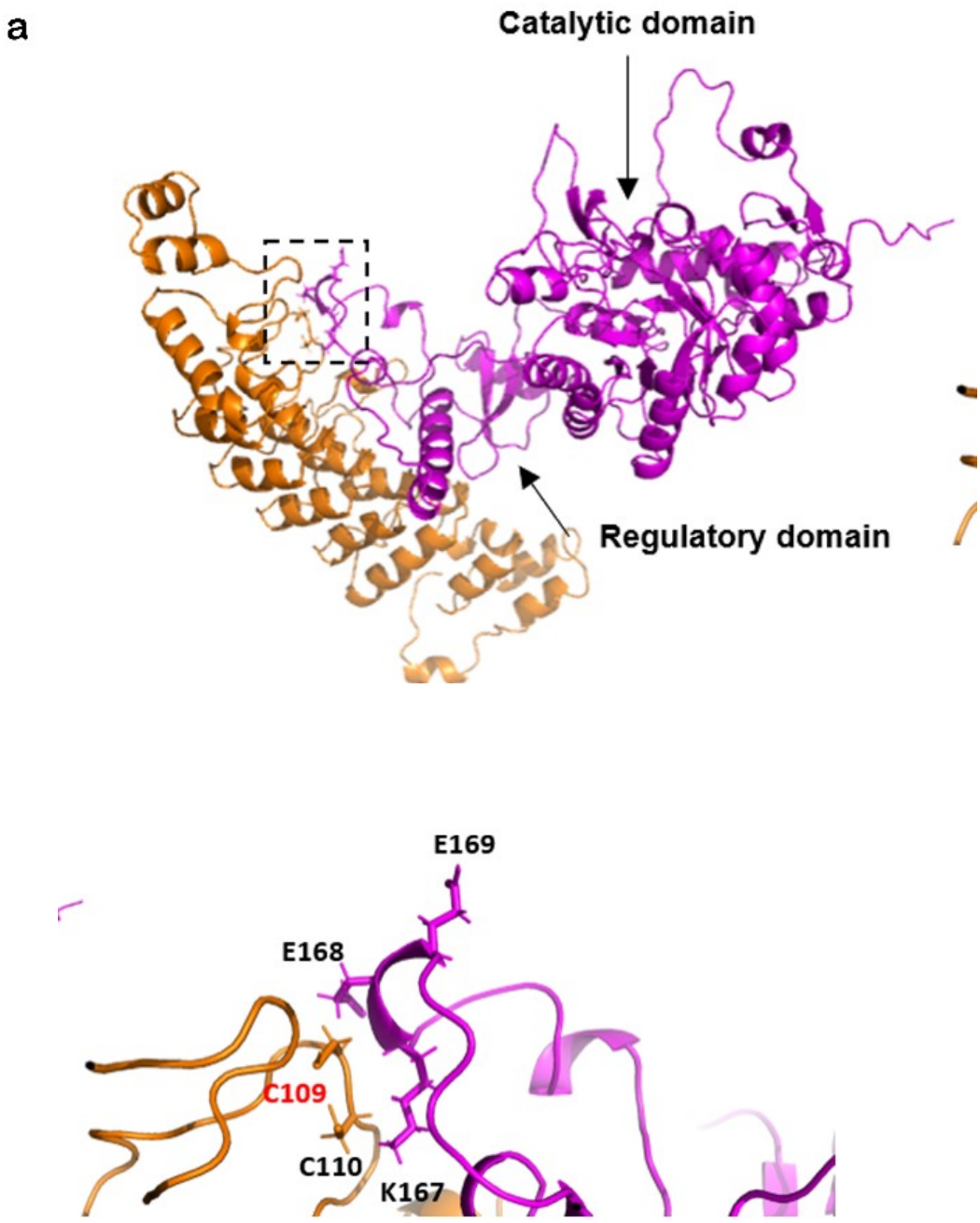
a
Catalytic domain
Regulatory domain
E169
E168
C109
C110
K167

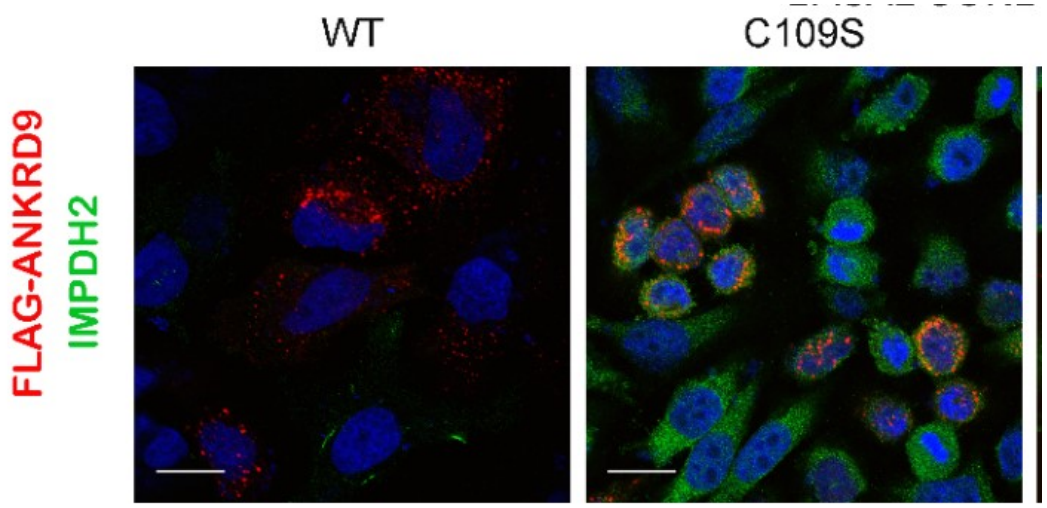
WT
C109S
FLAG-ANKRD9
IMPDH2

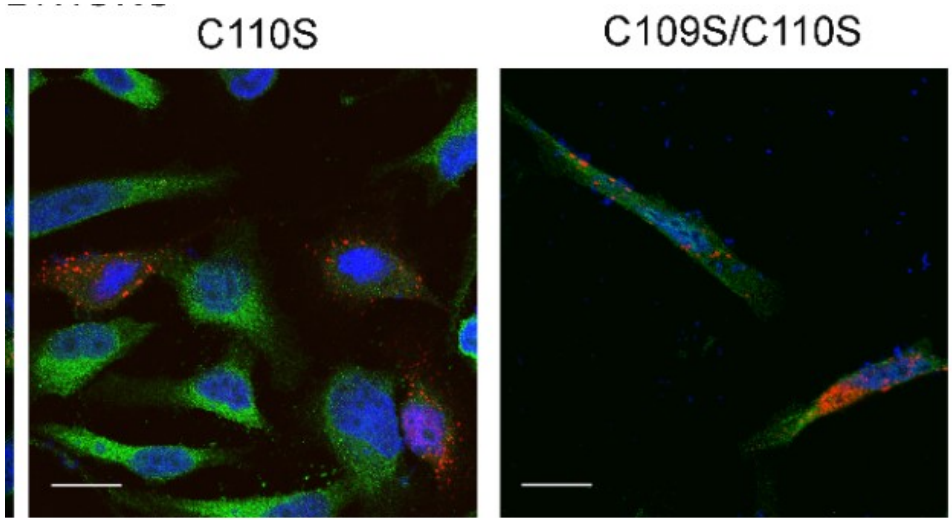
C110S
C109S/C110S

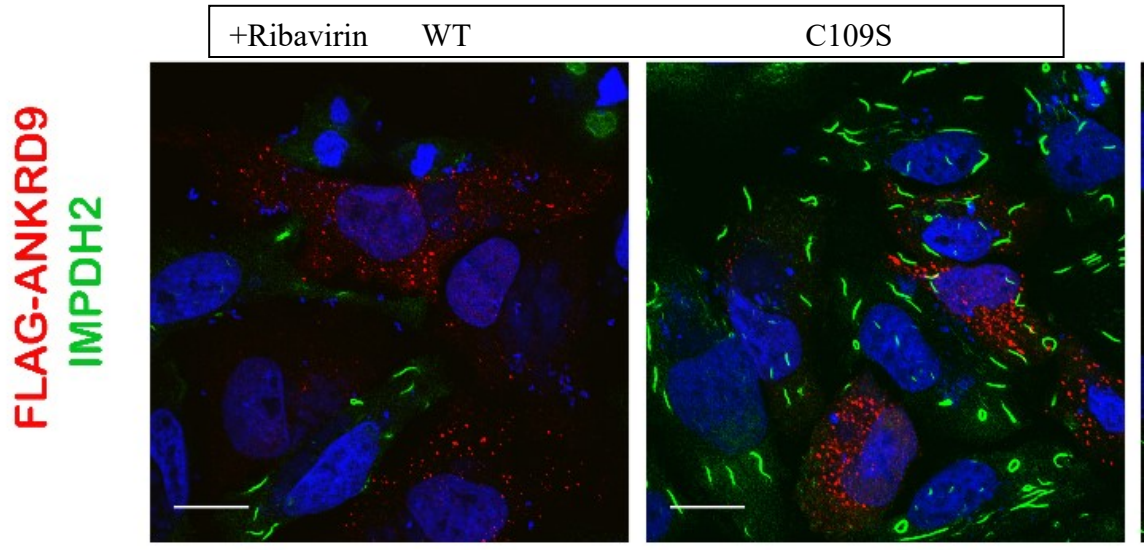
+Ribavirin
WT
C109S
FLAG-ANKRD9
IMPDH2

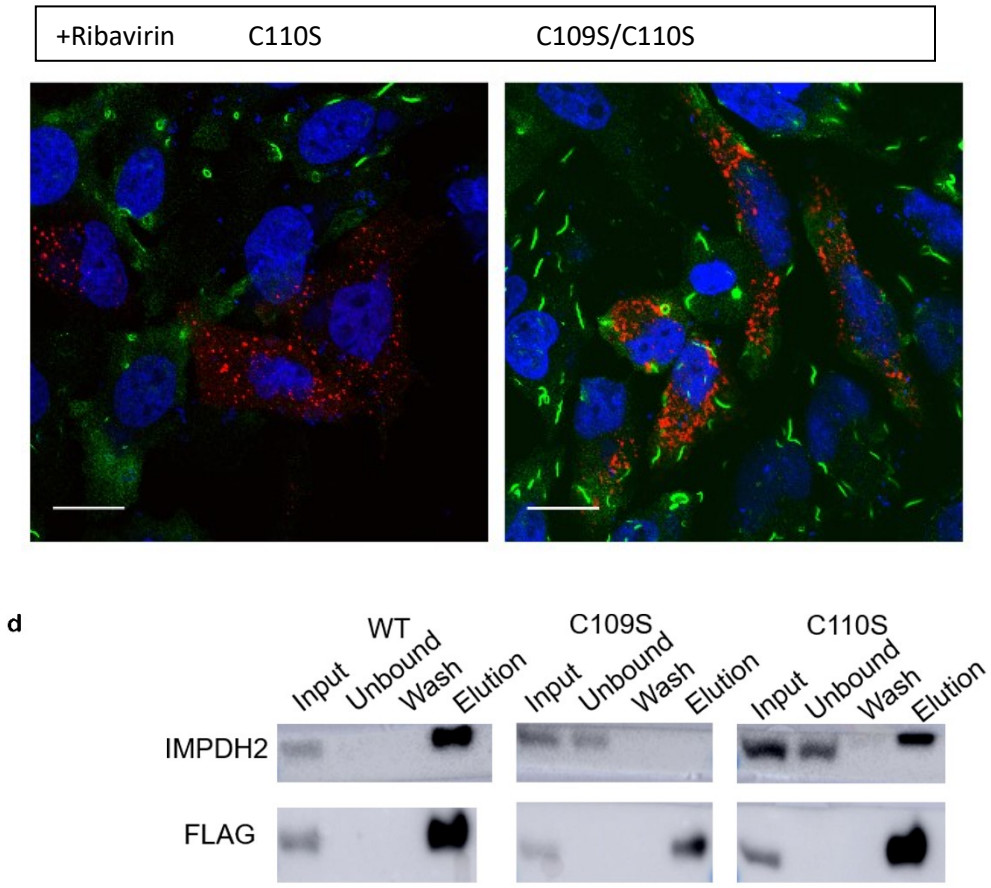

Figure 12: The Cys109 Cys110 motif contributes to ANKRD9-IMPDH2 interaction (a) *Left:* Docking model of ANKRD9 and IMPDH2 (PDB ID 1nf7) with the IMPDH2 catalytic and regulatory domains indicated by the arrows; the predicted interaction site is outlined by the box. *Right:* The magnified view of the predicted interaction site between ANKRD9 (orange) and IMPDH2 (purple). The CysCys motif in ANKRD9 interacts with K167, E168 and E169 of IMPDH2; (b) Cys mutants do not facilitate IMPDH2 degradation. HeLa cells were transfected with the WT ANKRD9 and indicated mutants under basal conditions and immunostained for FLAG and IMPDH2. Cells expressing WTANKRD9 showed significantly reduced IMPDH2 staining, whereas cells with the Cys mutants did not; n=3 (c) Cys mutants of ANKRD9 do not form rods with IMPDH2. HeLa cells were transfected with the indicated constructs and subsequently treated with 10 μM Ribavirin for 1hr prior to

immuno-staining for FLAG and IMPDH2; n=3 (d) The WT and ANKRD9 mutants were expressed in HeLa cells and

immunoprecipitated using Anti-FLAG M2 resin overnight. The next day the resin was washed and incubated with FLAG peptide at 2 mg/mL to elute. Input (10% ot total), unbound, wash, elution samples (40% of total) were western blotted for FLAG and IMPDH2, n=3.

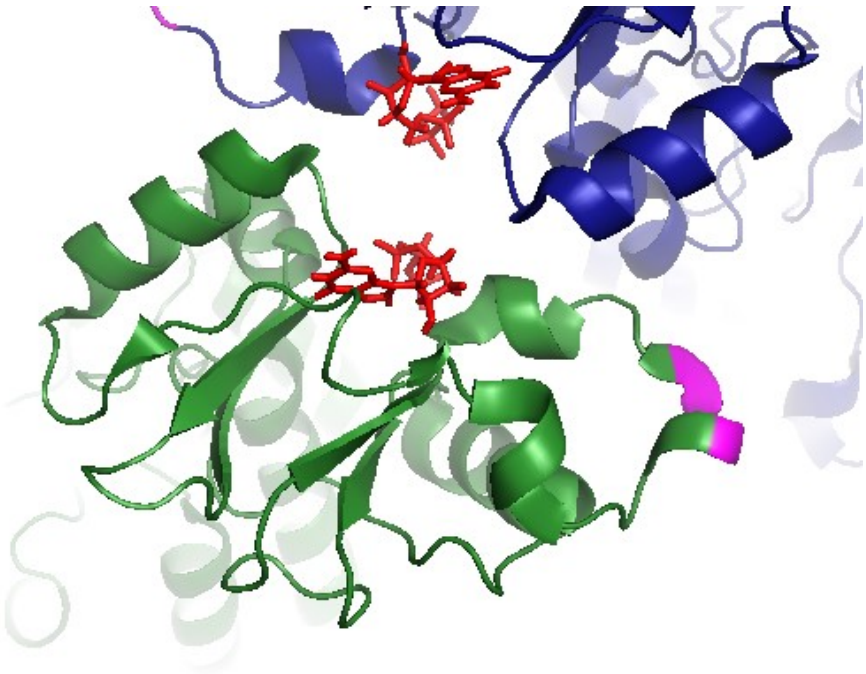

Figure 13: ANKRD9 binds IMPDH2 near nucleotide binding site. ANKRD9 is predicted to bind to IMPDH2 regulatory domain in the vicinity of the GDP/GTP binding site. Regulatory domains of IMPDH2 dimer (PDB ID 6I0M) are shown in green and blue; GTP is in red, the K167/E168/E169 motif (that is predicted to interact with the ANKRD9 CysCys-containing loop), is colored in pink.

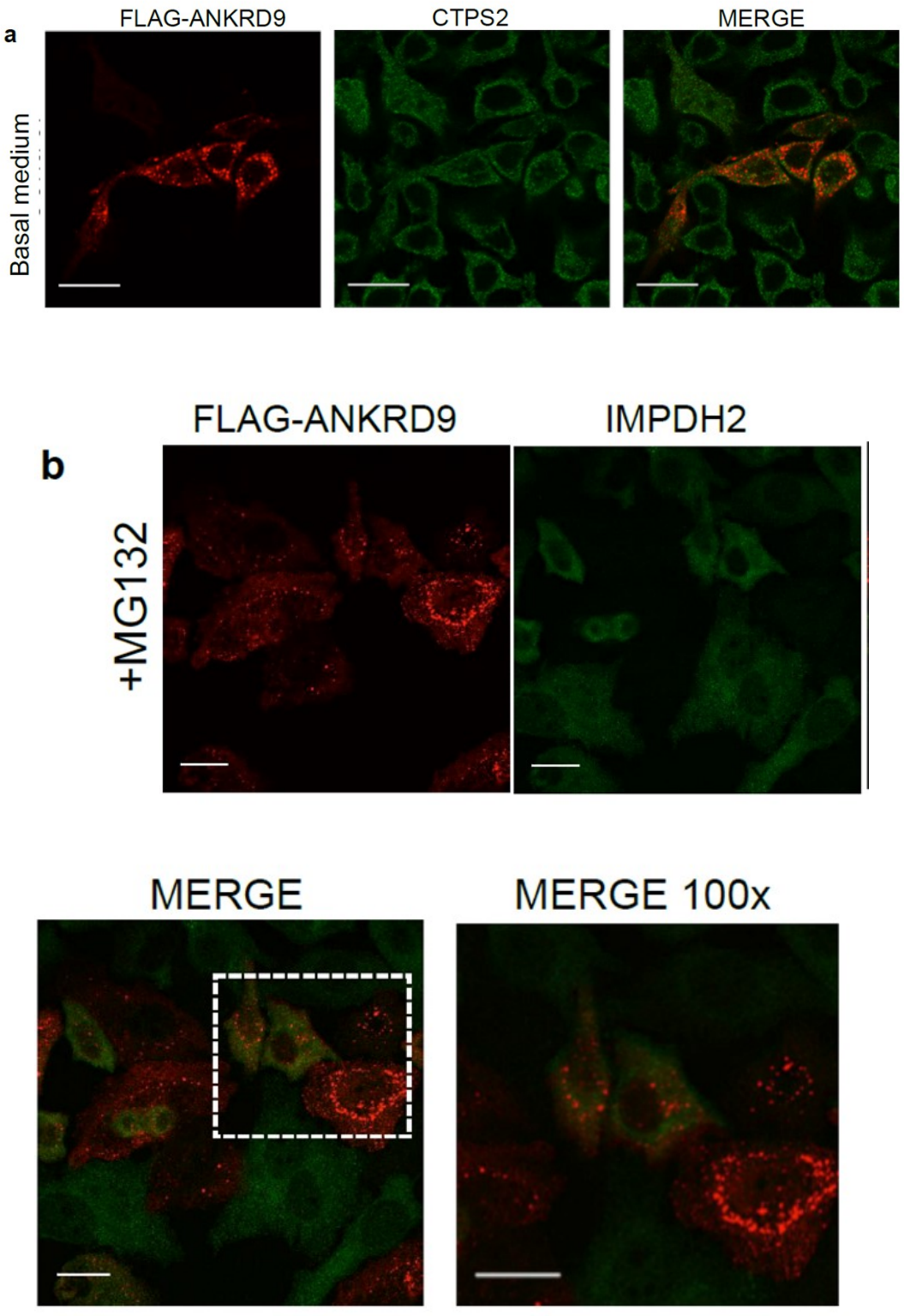
a
FLAG-ANKRD9
CTPS2
MERGE
Basal medium
b
FLAG-ANKRD9
IMPDH2
+MG132
MERGE
MERGE 100x

Figure 14: ANKRD9 and IMPDH2 interactions are specific (a) HeLa cells were transfected with FLAG-ANKRD9 and immunostained for FLAG and CTPS2 under basal growth conditions (10%FBS). Expression of ANKRD9 does not alter CTPS2 pattern/abundance, in contrast to IMPDH2 (see Fig 7b), which is markedly diminished under the same conditions; n=2 (b) HeLa cells were transfected with FLAG-ANKRD9, treated with 10 μM proteasome inhibitor MG132 for 4 hrs and stained for FLAG and IMPDH2. MG132 partially restores IMPDH2 staining in cells transfected with ANKRD9 as evidenced in insert where two out of the three cells have restored IMPDH2 staining. Scale bar: 20 μm

In contrast to WT ANKRD9, the C109S and C109S/C110S mutants did not significantly affect IMPDH2 levels (Fig 12b). Treatment with 10 μM Ribavirin for 1h confirmed the difference in IMPDH2 abundance between cells expressing the WT and mutant ANKRD9s; IMPDH2 rods were absent in cells expressing WT ANKRD9 mutants (Figure 12c). This reflected the marked decrease in IMPDH2 abundance, and present in cells with C109S and C109S/C110S variants. The effects of C110S mutant were less pronounced that those of the C109S, C109S/C110S variants and were closer to WT ANKRD9. This result suggested that Cys109 plays the primary role in interactions with IMPDH2.

This conclusion was confirmed by immunoprecipitation: unlike the WT ANKRD9, the C109S mutant did not pull down IMPDH2 (Fig. 12d). Taken together, these results suggest that under basal conditions excess ANKRD9 binds to IMPDH2 and negatively affects its abundance. Under condition of nutrient deprivation ANKRD9 loses ability to bind to vesicles, but retains ability to bind to IMPDH2 in rods. In rods, ANKRD9-dependent degradation of IMPDH2 is blocked, presumably by the tertiary structure of rods. Thus, the $Cys^{109}Cys^{110}$ motif plays an important role in both nutrient sensing and binding/regulation of IMPDH2.

ANKRD9 knockdown increases IMPDH2 levels and reduces rod formation under nutrient limiting conditions.

The above experiments provided evidence for the impact of elevated ANKRD9 on IMPDH2. To better understand how variation in ANKRD9 abundance affects IMPDH2 we decreased levels of ANKRD9 in HEK293A cells using siRNA. HEK293 cells were chosen because they express ANKRD9 at higher levels than HeLa cells and this allows more accurate measurements of siRNA-mediated down-regulation. HEK293 cells also show IMPDH2 assembly in rods upon serum starvation and the recombinant Flag-ANKRD9 has the same vesicular pattern under basal conditions as in HeLa cells (Fig. 15).

The siRNA-mediated knockdown reduced ANKRD9 mRNA levels by about 60% (Fig. 15a, upper panel); the protein levels could not be measured due to low sensitivity of available antibodies. The cells were then examined under basal and low serum conditions. ANKRD9 down regulation increased IMPDH2 expression levels (Fig. 16a, lower panel), in agreement with a previous report (42). Despite upregulation, IMPDH2 did not form rods in response to nutrient limitation in cells with down-regulated ANKRD9 (Fig 16b). This finding suggests that ANKRD9 serves to stabilize IMPDH2 rods when nutrients (presumably GTP pools) are depleted (Fig. 16d).

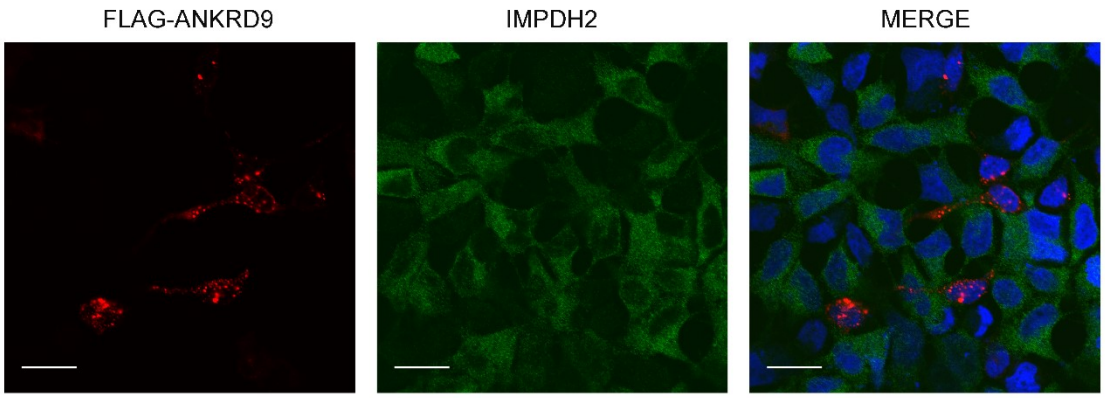

Figure 15: Recombinant ANKRD9 shows vesicular pattern and decreases IMPDH2 staining HEK293A cells were transfected with FLAG-ANKRD9 under basal conditions and immunostained for FLAG and IMPDH2. Cells expressing ANKRD9 (red) lack IMPDH2 staining (green), n=2 Scale bar: 20 μm.

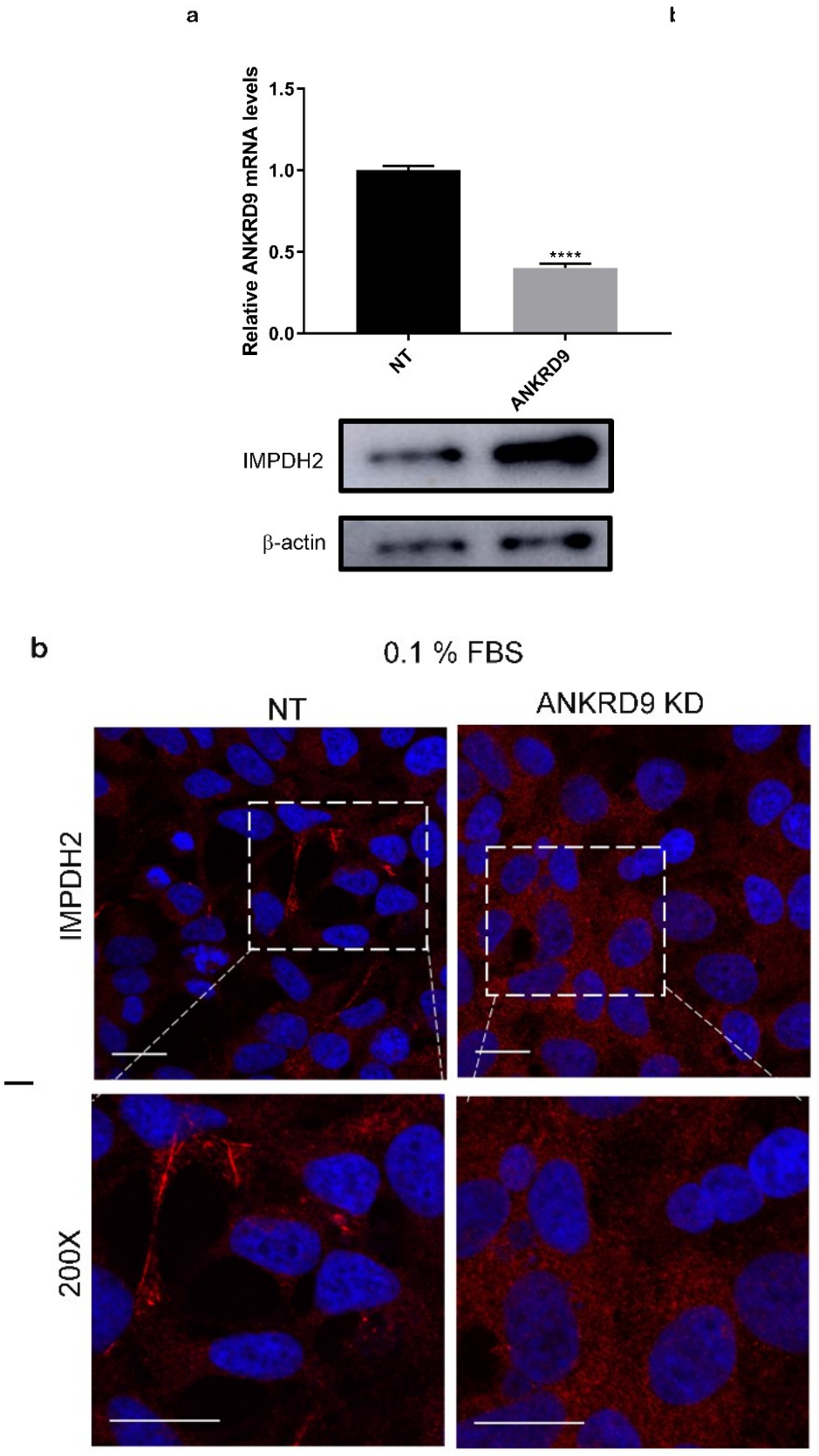
a
Relative ANKRD9 mRNA levels
1.5
1.0
0.5
0.0
****
NT
ANKRD9
IMPDH2
β-actin
b
0.1 % FBS
NT
ANKRD9 KD
IMPDH2
200X

c

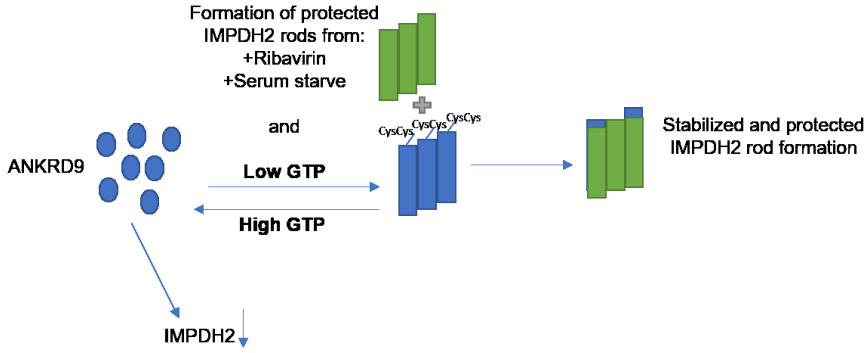

Figure 16: ANKRD9 knockdown increases IMPDH2 expression and reduces rod formation under nutrient limiting conditions. (a) HEK293A cells were transfected with non-targeted (NT) siRNA and ANKRD9 siRNA and ANKRD9 mRNA levels were quantified (top panel). IMPDH2 levels in corresponding cells were analyzed by western blot, β-actin was used as a loading control (lower panels). Decrease in ANKRD9 levels is associated with higher IMPDH2 abundance, n =3. (b) ANKRD9 down-regulation diminishes IMPDH2 rod formation under nutrient limitation. HEK293A cells were transfected with the indicated siRNAs and stained for IMPDH2 after cells were incubated in 0.1% FBS for 48 hours. IMPDH2 rods were apparent in control cells, no IMPDH2 rods are visible in cells treated with ANKRD9 siRNA, n = 3 (c) Cartoon showing that ANKRD9 forms rods with inhibited IMPDH2 when GTP pools are lowered and stabilizes IMPDH2 rod formation.

Section 2.4: Discussion

ANKRD9 is a highly conserved protein found in all vertebrates. The cellular and physiologic functions of ANKRD9 are poorly understood, and the limited available data paint a complex and confusing picture. The first report, published in 2009, found ANKRD9 mRNA levels to be responsive to changes in lipid metabolism and nutritional availability, whereas the second report, published in 2018, provided evidence that ANKRD9 could be involved in proteasomal degradation of IMPDH2, a nucleotide processing enzyme (40,42). Our laboratory previously identified ANKRD9 as a novel regulator of copper homeostasis based on specific elevation of cellular copper in response to ANKRD9 knockdown (37). These ANKRD9-influenced processes have little in common; to modulate these distinct pathways ANKRD9 is likely to interact with more than one cellular target and these interactions can be spatially, temporarily, and metabolically controlled. Here we show that ANKRD9 has at least 2 distinct intracellular locations: vesicles and cytosolic rods (Fig. 16c). The presence of ANKRD9 in these locations depends on metabolic state of the cell, and has distinct consequences for IMPDH2 abundance and macro-assembly. We have generated the molecular model for ANKRD9 and identified the cysteines residues required for changes in ANKRD9 intracellular localization and activity towards IMPDH2.

When cells are grown in low serum, ANKRD9 forms rods that overlap with IMPDH2 rods. While low serum condition can be used to block cell cycle, we suggest that ANKRD9 senses nutrient depletion rather than inhibition of the cell cycle progression. Our reasoning is the following. First, formation of rods takes longer than inhibition of cell cycle progression. Second, prolonged inhibition of IMPDH2 with Ribavirin accelerates formation of ANKRD9 rods suggesting that the transition of ANKRD9 from vesicle to rods is triggered by IMPDH2-

dependent nucleotide misbalance (compare Fig. 7a and 7b). Third, addition of guanosine rapidly disassembles ANKRD9 rods, suggesting that in low serum cellular guanine pools are lowered (Fig. 9).

The assembly into rods and rings is a characteristic property of IMPDH2 that has been extensively studied (58,59,61,62). This macro-assembly occurs in response to various triggers, including IMPDH2 inhibition, signaling during T-cell activation, or amino acid depletion. IMPDH2 has propensity for self-assembly and no proteins with enzymatic functions have been found to interact with IMPDH2 rods. GTP pools are critical for IMPDH rods formation, since guanosine but no other nucleosides reverse the macro-assembly (60,62,64,67). We found that guanosine also dis-assembles the ANKRD9/IMPDH2 complex and, significantly, restores ANKRD9 binding to vesicles. This observation suggests that ANKRD9 may sense levels of nucleotide pools and respond by changing its location/association with IMPDH2.

GTP and ATP bind to the regulatory domain of IMPDH2 and influence not only macro-assembly but also IMDPH2 activity (53-55,57). In our docking model, ANKRD9 interacts near the nucleotide-binding sites (Fig 13). This close proximity suggests that ANKRD9/IMPDH2 interaction in rods may influence nucleotide binding to IMPDH2, but this hypothesis requires further testing.

Our experiments show that ANKRD9 binds to the inhibited IMPDH2 and increases the length of IMPDH2 rods. The functional significance of IMPDH2 rods has been a subject of significant interest and debate in the literature, since the appearance of the rods is not linked to either IMPDH2 abundance or activity (both active and inhibited IMPDH2 form rods). Rods are readily formed in nutrient starved cells as well as in rapidly proliferating

cells, which may also have low surplus of nutrients. Our data suggest that under these circumstances macro-assembly into rods may protect IMPDH2 from ANKRD9-mediated degradation, which may otherwise occur when ANKRD9 loses association with vesicles in response to nutrient deprivation. ANKRD9 binding to IMPDH2 rods appears to stabilize them. In other words, the metabolic state of the cell determines whether ANKRD9 destroys or protects IMPDH2.

CTPS2 has been shown to form rods and rings. The CTPS2 rods are distinct from IMPDH2 rods although their assembly could be regulated by similar factors such as nucleotide metabolites (60). The previous proteome screen did not find CTPS2 among ANKRD9 binding partners (41) (only IMPDH1 and IMPDH2 were detected) and in our experiments we observed no effect of ANKRD9 on CTPS2, suggesting that the ANKRD9-IMPDH2 assembly and regulation is specific.

Comparison of the predicted ANKRD9 structure to structures of other better characterized ANKRD-containing proteins using 3D protein Blast show that three dimensional fold of ANKRD9 resembles that of the ankyrin binding domain of phospholipase iPLA2β as well as tankyrase. The homology to the latter enzyme is particularly interesting. Tankyrase mediates poly-ADP-ribosylation of various proteins, marking them for degradation via ubiquitin ligase pathway, and regulates mitosis, genome integrity, and cell signaling. As ANKRD9, tankyrase regulates protein abundance in various cellular locations; β-catenin in the cytosol and GLUT4 transporter in vesicles (30). It is tempting to speculate that coupling sensitivity to metabolites with changes in intracellular localization could be a common mechanistic feature of ANKRD-containing proteins with a structural similarity to ANKRD9.

Author contributions: DH and SL designed the experiments. DH and VK performed the experiments. DH, VK, IT, and HP analyzed the results. NMH provided critical reagents. DH wrote the paper with SL. We thank Dennis Chang for performing initial experiments that showed distinct ANKRD9 intracellular patterns. The Robetta server (http://**robetta**.bakerlab.org/) was used for the protein structure prediction.

Section 2.5: Methods

Cell lines—HeLa cells maintained in DMEM supplemented with 10% heat inactivated Fetal Bovine Serum (FBS), 1% Penicillin-Streptomycin and 1% non-essential amino acids and passaged every 2-3 days when cells were 80% confluent in T75 cm^2 flasks. HEK293A cells were maintained in DMEM supplemented with 10% Fetal Bovine Serum, 1% Penicillin-Streptomycin and 1% non-essential amino acids and passaged every 2-3 days when cells were 80% confluent in T75 cm^2 flasks.

Site-directed Mutagenesis in ANKRD9—An N-terminally labeled FLAG-tagged ANKRD9 construct was generated from the cDNA of human ANKRD9. This construct was cloned into a pcDNA3.1 vector containing blasticidin and ampicillin resistance. Mutations were introduced using the QuikChange XL mutagenesis kit. Primers were purchased from Integrative DNA technologies (IDT). Presence of correct mutations and the lack of unwanted mutations were verified by sequencing the coding region. Primers used for mutagenesis: C109S forward primer: 5'-AGCCG-CGCAGCTGCGGAAGCCGG-3'; C109S reverse primer: 5'-CCGGCTTCCGCAGCTGCGCGGCT-3'; C110S forward primer: 5'-GGGAGCCGCG-CTGCAGCGGAAGC-3'; C110S reverse primer: 5'-GCTTCCGCTGCAGCGCGGCTCCC-3'; C109S C110S forward primer: 5'- GGGAGCCG-CGCTGCTGCGGAAGCCGG-3'; C109S C110S reverse primer: 5'-CCGGCTTCCGCAGCAG-CGCGGCTCCC-3'

Immunofluorescence Microscopy—Cells were transfected with 1 μg FLAG-tagged ANKRD9 or FLAG-tagged ANKRD9 mutants using 2% Turbofect in 200 μL OPTI-MEM in 2 mL of 60% confluent cells on coverslips in 12-well plates for 16 hours and processed for

immunofluorescence as follows. HeLa cells were washed with PBS then fixed with 4% Formaldehyde for 15 minutes at RT. Cells were permeabilized with 0.1% Triton X-100 for 10 minutes with mild shaking. Cells were then blocked with 1% BSA, 1% gelatin in PBS overnight at 4 degrees C. The next day cells were incubated with primary antibody for one hour at RT in a humidified chamber. Mouse anti-FLAG was used at a DF (dilution factor) of 1:500, catalog number F1804; Millipore-Sigma, Rabbit anti-IMPDH2 was used at DF 1:300, catalog number ab75790; Abcam, Rabbit anti-CTPS2 was used at DF 1:300, catalog number ab235109; Abcam. Cells were then washed with PBS once, PBS+ 0.1% tween twice, then PBS, then incubated with fluorescent secondary antibody in the dark for one hour. Donkey anti-mouse AlexaFluor 555; catalog number A31570, Thermofisher, donkey anti-rabbit AlexaFluor 488, catalog number A21202, Thermofisher were used at DF 1:500. Donkey anti-rabbit AlexaFluor 555, catalog number ab150070, abcam, was used in Figure 15b. Coverslips were then washed as with primary with a final wash in water to remove excess salts. Coverslips were then mounted with fluoromount and DAPI at 50% each. Images were taken with an Olympus FV3000RS confocal microscope and processed using Fiji. Images in Figures 7 and 13 were taken with a Zeiss LSM 5 Pascal confocal microscope and processed using Image J.

Quantifying rod length—For rod length, images were processed as previously described (73). Briefly, images were deconvoluted to 8-bit and threshold was arbitrarily adjusted to 44 for all images. The analyze particles application was used where length below 0.5 was excluded and circularity to 1 was used. Total rod number was then compared to total cells in image to

obtain rod number per cell. Ten images in random locations containing at least ten cells was used for quantification in each category of non-transfected versus transfected conditions.

Structural modeling—Homology model: We used a crystal structure of protein IMPDH2 (PDB ID 1nf7) and the Robetta model for ANKRD9. To refill all missed regions of the IMPDH2 structure, we created a homology model using the Molecular Operating Environment (MOE) software, version 2018.01 (CCG, Montreal, Canada). The full sequence of the protein including missed in crystal structure amino acids was used. Homology models were created with the Homology Model application of Protein module, using Amber10: EHT forcefield with a Reaction Field (R-Field). A model with better RMSD and contact energy was chosen.

Docking: Docking of IMPDH2 and ANKRD9 was conducted with the Dock application of the Compute module in MOE. A number of docking configurations called poses were generated and scored. The score was calculated as a combination of free energy of binding including, among others contributions, solvation and entropy terms, and targeted regions interaction score that was calculated as a number of heavy atoms from the conserved regions of 6 sites in protein ANKRD9 contacting heavy atoms of protein IMPDH2.

siRNA knockdown of ANKRD9—siGENOME SMART pool constructs against human ANKRD9 (Catalog number M-015551-01-0005) was used in HEK293A cells. Wet-reverse transfection was performed as follows: Cells were grown to ~60% confluency in complete medium without antibiotics. DharmaFECT at 2.5% (Cat. T-2001-002, Dharmacon) and OPTI-MEM was mixed with 20 nM siRNA and OPTI-MEM, added to wells and incubated

for 30 minutes. $1.37x10^5$ cells/mL of HEK293A cells were then added and mixed with siRNA plus DharmaFECT and incubated at 37 degrees for 60 hrs. Complete medium without antibiotics was added for 12 hrs for a total of 72 hours incubation. Cells were then processed for RT-qPCR and immunostaining for IMPDH2 rod formation.

Real-time quantitative PCR (RT-qPCR)—RNA isolation and mRNA level quantitation were performed as previously described (83). RNA isolation was done with the RNAeasy kit (Qiagen), cDNA was generated and RT-PCR was done with the One-Step SYBR green kit (Applied Biosystems) on an ABI 7500 Sequence Detection System (Applied Biosystems). S18 was used for normalization for ΔΔCt analysis. Primers used in qPCR are as follows: S18 forward: 5'-TTCTGG-CCAACGGTCTAGACAAC-3'; S18 reverse: 5'-CCAGTGGTCTTGGTGTGCTGA-3'; ANKRD9 forward: 5'-CTGGTCACCGCCATCTCT-3'

ANKRD9 reverse: 5'-CTAGCCTTTGCCAGT-GAGGT-3'

Co-Immunoprecipitation and Western Blotting— HeLa cells were transfected with FLAG-tagged ANKRD9 and lysed with 1X RIPA buffer in PBS. Lysates were cleared with centrifugation at 10,000 RPM for 10 minutes. Supernatants were used in western blotting and co-immunoprecipitation. For the latter 15 μL Anti-FLAG M2 resin (catalog number A2220, Millipore-Sigma) was washed with PBS then 500 μL lysate was loaded onto resin via batch purification and incubated overnight with rotation. Resin was washed twice with PBS then incubated with 60 μL of 2 mg/mL of FLAG peptide (catalog number F4799, Millipore-Sigma) for 2 hrs with rotation. Supernatant was collected and analyzed via western blot.

Samples from input, unbound, wash an elution were taken to be analyzed. For western blotting the following antibody dilutions were used: Mouse Anti-FLAG, dilution factor 1:10,000, Rabbit anti-IMPDH2, dilution factor 1:10,000, Rabbit anti-CTPS2, dilution factor 1:10,000, Mouse anti-Beta Actin, dilution factor 1:10,000 Catalog number NB600-501, purchased from Novus. Standard gel running and transfer methods were used, membranes were blocked for 1hr in 5% milk in PBS at RT and incubated with primary antibody in 1% milk in PBS-T. Membranes were washed the next day in PBS-T and incubated with HRP-conjugated secondary antibody, dilution factor 1:10,000 for 1hr at RT and imaged with chemiluminescence.

Chapter 3: Conclusions and future directions

Section 3.1: Summary and conclusions

Section 3.2 Future Directions

Chapter 3: Conclusions and future directions

Section 3.1: Summary and conclusions

Metabolic state governs transition between ANKRD9 rods and vesicles

We have shown that ANKRD9 has two distinct cellular forms whose transition is mediated by cells metabolic state. The switch between two forms involves depletion of nutrients: incubating cells for 48 hours in 0.1 % FBS converted the majority of ANKRD9 from being associated with vesicles to forming rod structures. These rods co-localize with IMPDH2, a known rod assembly enzyme that catalyzes the rate-limiting step of guanine nucleotide biosynthesis. We have also shown that the guanosine metabolite rapidly reverts ANKRD9 to vesicles under otherwise nutrient deprived conditions. That guanosine converts rods back to vesicles suggests that ANKRD9 and IMPDH2 are regulated by similar factors and that perhaps GTP can directly bind ANKRD9. This hypothesis is further supported by the presence of nucleotide binding pocket predicted in our ANKRD9 model. Effect of metabolites on ANKRD9 behavior comes hand-in-hand with the first ANKRD9 report where a fasting-refeeding model increased mRNA levels of ANKRD9. Taken together, the available data strongly suggest that the dynamic nature of ANKRD9 is due to metabolic state of a cell.

ANKRD9 stabilizes IMPDH2 rods

ANKRD9 rods formed under nutrient deprivation fully co-localize with IMPDH2 rods but not with CTPS2, which suggest a specific role of ANKRD9 in IMPDH2-dependent pathways. In addition, ANKRD9 rods co-localize specifically with inhibited IMPDH2 rods; when cells are pre-treated with substrate inhibitor Ribavirin rod length increases with

ANKRD9 overexpression and rod number decreases. In addition, ANKRD9 knockdown increases IMPDH2 levels but lowers the formation of rods upon nutrient deprivation. These results suggest that ANKRD9 presence rather than IMPDH2 abundance is a determining factor for formation of IMPDH2 rods under condition of nutrient depletion. In contrast, under basal conditions ANKRD9 overexpression lowers IMPDH2 levels in agreement with a previous report suggesting that ANKRD9 is a part of a ubiquitin ligase complex that specifically targets IMPDH2. In other words, there must be a delicate balance between having enough ANKRD9 available to stabilize IMPDH2 rods under particular metabolic conditions but not too much ANKRD9 as it lowers IMPDH2 levels.

Section 3.2 Future Directions

Guanosine control of ANKRD9 cellular forms

Guanosine reversal and a predicted nucleotide binding pocket in ANKRD9 (our data) suggest that ANKRD9 rods may be controlled by nucleotide metabolism. To this end, mutagenizing residues in the predicted binding pocket may help to determine whether ANKRD9 binds GTP as a prerequisite to rod dispersal and return to vesicles. The residues we have mutated, a conserved CysCys motif, influence both rod formation and interactions with IMPDH2. Identifying mutants that allow ANKRD9 to form guanosine-insensitive rods would help to further investigate ANKRD9 function and mechanism.

In addition, we have noticed that IMPDH2 residues that are predicted to interact with the CysCys motif of ANKRD9 are disordered in the crystal structure of IMPDH2 when the latter has bound GDP versus GTP. This suggests that GTP binding may indeed critically affect the IMPDH2/ANKRD9 interface and thus govern the reversal of ANKRD9 from rods

to vesicles. Future work on the mechanism of this process would be accelerated by having structures of ANKRD9 and ANKRD9/IMPDH2 complex, as well as by direct measurements of nucleotide binding to purified ANKRD9 and its complex with IMPDH2. Additionally, visualizing ANKRD9-dependent rod formation with electron microscopy would help to clarify the significant scale discrepancy between the rods formed by purified IMPDH2 (which are typically 200-300 nanometers) to those seen in microscopy in cells (3-5 microns).

Copper relation and in vivo ANKRD9 studies

In our laboratory, initial studies into ANKRD9 came from its discovery as a novel copper regulator whose knockdown specifically and significantly increased copper levels. This finding was interesting, because in the literature ANKRD9 was reported as a regulator of fat metabolism and the link between copper and fat balance has recently emerged. Characterization of ANKRD9 knockout mice (available through KOMP consortium; http://www.informatics.jax.org/allele/MGI:4419197) would further these studies and may provide better understanding of how multiple roles of ANKRD9 are interconnected. ANKRD9-/- mice are viable with deceased body fat and increased lean body mass which is in line with the initial report on ANKRD9 having a role in lipid metabolism. Analysis of mouse metabolism during development would help clarify ANKRD9's role in both copper metabolism and lipid homeostasis. Also, because of the copper phenotype found in cells it is possible that older ANKRD9-/- mice may develop pathologies related to copper overload . Lastly, primary cells from these knockout mice could be used for IMPDH2 studies to confirm the requirement for ANKRD9 in rod formation and possible increases in protein abundance.

The above studies would give structural and *in vivo* data supporting the determined role of ANKRD9 in IMPDH2 abundance and macroassembly and the earlier determined role of ANKRD9 in copper metabolism. This would be intriguing as it would show two separate roles for this adaptor protein which are most likely connected through as of now unknown means.

Appendix

Section 1.1: Glutamine modulates ANKRD9 transition to rods

Section 1.2: ANRKD9 co-localizes with the ERGIC53 marker

Appendix

Section 1.1: Glutamine modulates ANKRD9 transition to rods

Previous studies of factors that trigger formation of IMPDH2 rods have shown that glutamine deprivation, whereby glutamate is broken down into α-ketoglutarate and ammonia by glutamate dehydrogenase (50,66,84), causes rod formation (48). Interestingly, this phenotype was suppressed with low FBS levels in growth medium. These results suggest that metabolic state indeed governs the transition to rods, even in IMPDH2. We therefore tested whether ANKRD9 responded to media not containing glutamine under both 10% and 0.1% FBS conditions. Surprisingly, ANKRD9/IMPDH2 rods did not form under 0.1% FBS with DMEM that did not contain glutamine for 48 hours. These results point to a potential role for glutamine in the transition of ANKRD9 from vesicles to rods as well as a possible explanation as to why the cysteine mutants do not form vesicles. Cysteines can be oxidized or reduced depending on the redox state of the cell where glutamine plays a significant role in glutathione metabolism; without glutamine the cell can enter an oxidized state from lowered production of glutathione (39,50). This suggests that the tandem cysteine residues in ANKRD9 may need to be in a reduced state to allow rod formation to occur.

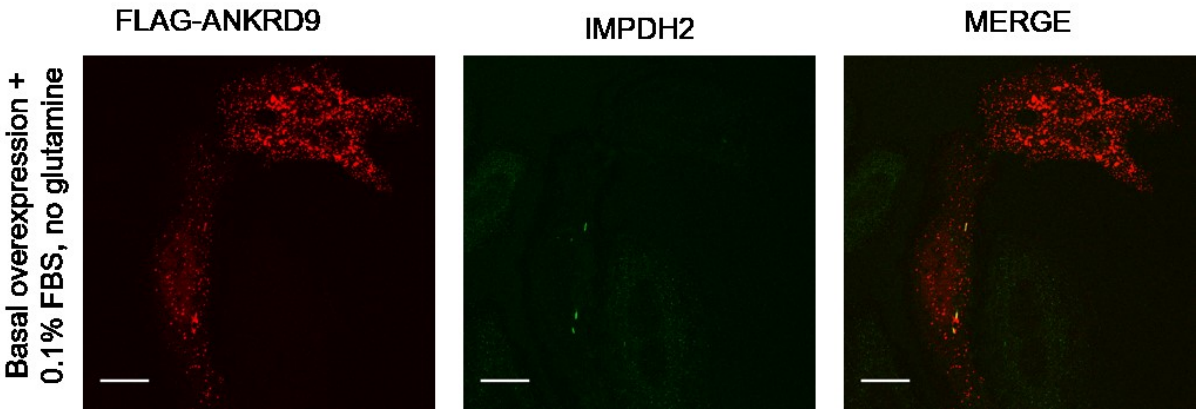

Figure 17: Glutamine prevents rod formation under nutrient limiting conditions. HeLa cells were transfected with FLAG-ANKRD9 in glutamine free media then placed in 0.1% FBS for 48 hours and stained for FLAG and IMPDH2. As previously reported, IMPDH2 forms rods under these conditions (48) but here ANKRD9 stays in vesicular form. Scale bar: 20 μm .

Section 1.2: ANRKD9 co-localizes with the ERGIC53 marker

The previous report from our laboratory identified ANKRD9 as a possible regulator of copper metabolism (37) as well as normal Golgi morphology (unpublished result). An earlier report also suggested that under basal condition ANKRD9 is targeted to vesicles (40). To better understand localization and function of ANKRD9 under basal conditions we carried out co-localization studies with various organelle markers. Markers tried included TGN-46 (ab16049, abcam), Golgin 97 (ab84340, abcam), LAMP1 for lysosomes (Rat anti-LAMP1 was used but was inconclusive, ab108597, Abcam) and ERGIC53 (sc-32442 Santa Cruz). These experiments revealed that the ANKRD9 vesicular form co-localizes with ERGIC53 (Figure 18) and may alter this compartments state. ERGIC53 marks an ER-Golgi compartment where membrane budding and vesicle fusion constantly takes place. Further studies examined outer coat protein Sec31 where a 'neighboring' effect (not colocalized but next to each other) occurred with ANKRD9 vesicles; here ANKRD9 does not co-localize with COPII vesicles. Sec31 usually pairs with Sec13 but staining with this antibody was inconclusive. These results suggest that ANKRD9 may be involved with trafficking and perhaps modification of proteins along the secretory pathway.

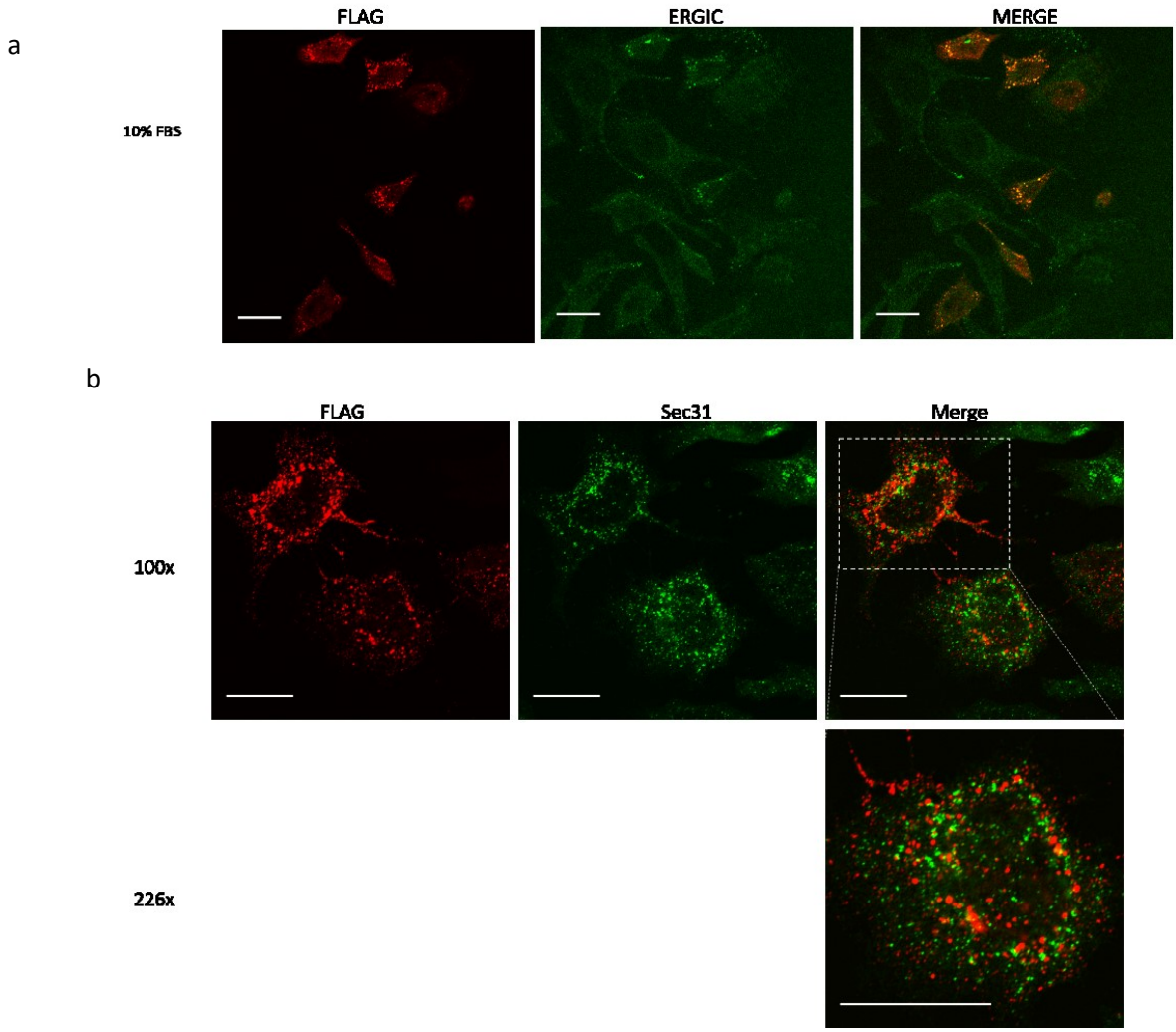

Figure 18: ANRKD9 co-localizes with ERGIC53 and neighbors Sec31(a) HeLa cells were transfected with FLAG-ANKRD9 under basal conditions (10% FBS) then immunostained for FLAG and ERGIC53 (b) HeLa cells were transfected with FLAG-ANKRD9 and stained for FLAG and Sec31. Lower panel is a close up view of the neighboring effect of ANKRD9 and Sec31, suggesting a role in trafficking, specifically in the outer coat membrane. Scale bar: 20 μm.

Bibliography:

1. Graham, T. A., Ferkey, D. M., Mao, F., Kimelman, D., and Xu, W. Tcf4 can specifically recognize beta-catenin using alternative conformations.
2. Bell, J. K., Botos, I., Hall, P. R., Askins, J., Shiloach, J., Segal, D. M., and Davies, D. R. (2005) The molecular structure of the Toll-like receptor 3 ligand binding domain. *PNAS* **102**, 109676-110980
3. Islam, Z., Nagampalli, R. S. K., Fatima, M. T., and Ashraf, G. M. (2018) New paradigm in ankyrin repeats: Beyond protein-protein interaction module. *International Journal of Biological Macromolecules* **109**, 1164-1173
4. Tewari, R., Bailes , E., Bunting, K. A., and Coates, J. C. (2010) Armadillo-repeat protein functions: questions for little creatures. *Trends in Cell Biology* **20**, 470-481
5. Sedgwick, S. G., and Smerdon, S. J. (1999) The ankyrin repeat: d diversity of interactions on a common structural framework. *Trends in Biochemical Sciences* **24**, 311-316
6. Mosavi, L. K., Cammett, T. J., Desrosiers, D. C., and Peng, Z.-Y. (2004) The ankyrin repeat as molecular architecture for protein recognition. *Protein Science* **13**, 1435-1448
7. Li, J., Mahajan, A., and Tsai, M.-D. (2006) Ankyrin Repeat: A Unique Motif Mediating Protein-Protein Interactions. *Biochemistry* **45**, 15168-15178
8. Zhu, Y., Kakinuma, N., Wang, Y., and Kiyama, R. (2008) Kank proteins: A new family of ankyrin-repeat domain-containing proteins. *Biochimica et Biophysica Acta* **1780**, 128-133

9. Wang, H.-l., Fan, S.-s., Pang, M., Liu, Y.-h., Guo, M., Liang, J.-b., Zhang, J.-l., Yu, B.-f., Guo, R., Xie, J., and Zheng, G.-p. (2015) The Ankyrin Repeat Domain 49 (ANKRD49) Augments Autophagy of Serum-Starved GC-1 Cells through the NF-kB Pathway. *PLoS ONE* **10**

10. Ling, S. S. M., Chen, Y.-T., Wang, J., Richards, A. M., and Liew, O. W. (2017) Ankyrin Repeat Domain 1 Protein: A functionally Pleiotropic Protein with Cardiac Biomarker Potential. *International Journal of Molecular Sciences* **18**

11. Takahashi, N., Hamada-Nakahara, S., Itoh, Y., Takemura, K., Shimada, A., Ueda, Y., Kitamata, M., Matsuoka, R., Hanawa-Suetsugu, K., Senju, Y., Mori, M. X., Kiyonaka, S., Kohda, D., Kitao, A., Mori, Y., and Suetsugu, S. (2014) TRPV4 channel activity is modulated by direct interaction of the ankyrin domain to $PI(4,5)P_2$. *Nature Communications* **5**

12. Michaely, P., Tomchick, D. R., Machius, M., and Anderson, R. G. W. (2002) Crystal structure of a 12 ANK repeat stack from human ankyrinR. *The EMBO Journal* **21**, 6387-6396

13. Mosavi, L. K., Minor, J., Daniel L., and Peng, Z.-y. (2002) Consensus-derived structural determinants of the ankyrin repeat motif. *Proceedings of the National Academy of Sciences* **99**, 16029-16034

14. Kengyel, A., Becsi, B., Konya, Z., Sellers, J. R., Erdodi, F., and Nyitrai, M. (2015) Ankyrin domain of myosin 16 influences motor function and decreases protein phosphatase catalytic activity. *European Biophysics Journal* **44**, 207-218

15. Chaves-Sanjuan, A., Barrena-Sanchez, M. J., Gonzalez-Rubio, J. M., and Albert, A. (2014) Preliminary crystallographic analysis of the ankyrin-repeat domain of

Arabidopsis thaliana AKT1: identification of the domain boundaries for protein crystallization. *Acta Crystallographica* **F70**, 509-512

16. Tripp, K. W., and Barrick, D. (2008) Rerouting the Folding Pathway of the Notch Ankyrin Domain by Reshaping the Energy Landscape. *Journal of the American Chemical Society* **130**, 5681-5688
17. Zweifel, M. E., Leahy, D. J., Hughson, F. M., and Barrick, D. (2009) Structure and stability of the ankyrin domain of the *Drosophila* Notch receptor. *Protein Science* **12**, 2622-2632
18. Kline, C. F., Scott, J., Curran, J., Hund, T. J., and Mohler, P. J. (2014) Ankyrin-B Regulates $Ca_v2.1$ and $Ca_v2.2$ Channel Expression and Targeting. *The Journal of Biological Chemistry* **289**, 5285-5295
19. Abdel-Rahman, N., Martinez-Arias, A., and Blundell, T. L. (2011) Probing the druggability of protein-protein interactions: targeting the Notch1 receptor ankyrin domain using a fragment-based approach. *Biochemical Society Transactions* **39**, 1327-1333
20. Ipsaro, J. J., Huang, L., and Mondraon, A. (2009) Structures of the spectrin-ankyrin interaction binding domains. *Blood* **113**, 5385-5393
21. Zhang, Z., Devarajan, P., Dorfman, A. L., and Morrow, J. S. (1998) Structure of the Ankyrin-binding Domain of alpha-Na,K-ATPase. *The Journal of Biological Chemistry* **273**, 18681-18684
22. Gonzalo Parra, R., Espada, R., Verstraete, N., and Ferreiro, D. U. (2015) Structural and Energetic Characterization of the Ankyrin Repeat Protein Family. *PLoS Computational Biology* **11**

23. Chakrabarty, B., and Parekh, N. (2014) Identifying tandem Ankyrin repeats in protein structures. *BMC Informatics* **15**

24. Kozlov, G., Wong, K., Wang, W., Skubak, P., Munoz-Escobar, J., Liu, Y., Siddiqui, N., Pannu, N. S., and Gehring, K. (2018) Ankyrin repeats as a dimerization module. *Biochemical and Biophysical Research Communications* **495**, 1002-1007

25. Inada, H., Procko, E., Sotomayor, M., and Gaudet, R. (2012) Structural and Biochemical Consequences of Disease-Causing Mutations in the Ankyrin Repeat Domain of the Human TRPV4 Channel. *Biochemistry* **51**, 6195-6206

26. Lishko, P. V., Procko, E., Jin, X., Phelphs, C. B., and Gaudet, R. (2007) The Ankyrin Repeats of TRPV1 Bind Multiple Ligands and Modulate Channel Sensitivity. *Neuron* **54**, 905-918

27. Michel, F., Soler-Lopez, M., Petosa, C., Cramer, P., Siebenlist, U., and Muller, C. W. (2001) Crystal structure of the ankyrin repeat domain of Bcl-3: a unique member of the Ikb protein family. *The EMBO Journal* **20**, 6180-6190

28. Palmer, S., and Chen, Y. H. (2008) Bcl-3, a multifaceted modulator of NF-kB-mediated gene transcription. *Immunologic Research* **42**, 210-218

29. Riffell, J. L., Lord, C. J., and Ashworth, A. (2012) Tankyrase-targeted therapeutics: expanding opportunities in the PARP family. *Nature reviews Drug Discovery* **11**

30. Su, Z., Deshpande, V., James, D. E., and Stockli, J. (2018) Tankyrase modulates insulin sensitivity in skeletal muscle cells by regulating the stability of GLUT4 vesicle proteins. *The Journal of Biological Chemistry* **293**, 8578-8587

31. Leslie, C. C. (2015) Cytosolic phospholipase A_2: physiological function and role in disease. *The Journal of Lipid Research* **56**, 1386-1402

32. Tang, J., Kriz, R. W., Wolfman, N., Shaffer, M., Seehra, J., and Jones, S. S. (1997) A Novel Cytosolic Calcium-independent Phospholipase A_2 Contains Eight Ankyrin Motifs. *The Journal of Biological Chemistry* **272**, 8567-8575

33. Ramanadham, S., Ali, T., Ashley, J. W., Bone, R. N., Hancock, W. D., and Lei, X. (2015) Calcium-independent phospholipases A_2 and their roles in biological processes and diseases. *The Journal of Lipid Research* **56**, 1643-1668

34. Lio, Y.-C., and Dennis, E. A. (1998) Interfacial activation, lysophospholipase and transacylase activityof Group VI Ca^{2+}-independent phospholipase A_2. *Biochimica et Biophysica Acta (BBA) - Lipids and Lipid Metabolism* **1392**, 320-332

35. Balsinde, J., Balboa, M. A., and Dennis, E. A. (1997) Antisense Inhibition of Group VI Ca^{2+}- independent Phospholipase A_2 Blocks Phospholipid Fatty Acid Remodeling in Murine $P388D_1$ Macrophages. *The Journal of Biological Chemistry* **272**, 29317-29321

36. Herbert, S. P., and Walker, J. H. (2006) Group VIA Calcium-Independent Phospholipase A_2 Mediates Endotelial Cell S Phase Progression. *The Journal of Biological Chemistry* **281**, 35709-35716

37. Malinouski, M., Hasan, N. M., Zhang, Y., Seravalli, J., Lin, J., Avanesov, A., Lutsenko, S., and Gladyshev, V. N. (2014) Genome-wide RNAi ionomics screen reveals new genes and regulation of human trace element metabolism. *Nature Communications* **5**

38. Bhattacharjee, A., Yang, H., Duffy, M., Robinson, E., Conrad-Antoville, A., Lu, Y.-W., Capps, T., Braiterman, L., Wolfgang, M., Murphy, M. P., Yi, L., Kaler, S. G., Lutsenko, S., and Ralle, M. (2016) The Activity of Menkes Disease protein ATP7A Is

Essential for Redox Balance in Mitochondria. *The Journal of Biological Chemistry* **291**, 16644-16658

39. Lutsenko, S. (2016) Copper trafficking to the secretory pathway. *Metallomics* **8**, 840-852

40. Wang, X., Newkirk, R. F., Carre, W., Ghose, P., Igobudia, B., Townsel, J. G., and Cogburn, L. A. (2009) Regulation of ANKRD9 expression by lipid metabolic perturbations. *BMB reports* **42**, 568-573

41. Huttlin, E. L., Ting, L., Bruckner, R. J., Gebreab, F., Gygi, M. P., Szpyt, J., Tam, S., Zarraga, G., Colby, G., Baltier, K., Dong, R., Guarani, V., Pontano Vaites, L., Ordureau, A., Rad, R., Erickson, B. K., Wuhr, M., Chick, J., Zhai, B., Kolippakkam, D., Mintseris, J., Obar, R. A., Harris, T., Artavanis-Tsakonas, S., Sowa, M. E., De Camilli, P., Paulo, J. A., Harper, J. W., and Gygi, S. P. (2015) The BioPlex Network: A Systematic Exploration of the Human Interactome. *Cell* **162**, 425-440

42. Lee, Y., Lim, B., Lee, S. W., Lee, W. R., Kim, Y.-I., Kim, M., Ju, H., Kim, M. Y., Kang, S.-J., Song, J.-J., Lee, J. E., and Kang, C. (2018) ANKRD9 is assoicated with tumor suppression as a substrate receptor subunit of u. *BBA-Molecular Basis of Disease*

43. Shin, G., Kang, T.-W., Yang, S., Baek, S.-J., Jeong, Y.-S., and Kim, S.-Y. (2011) GENT: Gene Expression Database of Normal and Tumor Tissues. *Cancer Informatics* **10**, 149-157

44. Aaen Andresen, C., Smedegaard, S., Beck Sylvestersen, K., Svensson, C., Igleslas-Gato, D., Cazzamali, G., Nielsen, T. K., Nielsen, M. L., and Flores-Morales, A. (2014) Protein Interaction Screening for the Ankyrin Repeats and Suppressor of

Cytokine Signaling (SOCS) Box (ASB) Family Identify Asb11 as a Novel Endoplasmic Reticulum Resident Ubiquitin Ligase. *The Journal of Biological Chemistry* **289**, 2043-2054

45. Colby, T. D., Vanderveen, K., Strickler, M. D., Markham, G. D., and Goldstein, B. M. (1999) Crystal structure of human type II inosine monophosphate dehydrogenase: Implications for ligand binding and drug design. *PNAS* **96**, 3531-3536

46. Sintchak, M. D., and Nimmesgern, E. (2001) The structure of inosine 5'-monophosphate dehydrogenase and the design of novel inhibitors. *Immunopharmacology* **47**, 163-184

47. Sintchak, M. D., Fleming, M. A., Futer, O., Raybuck, S. A., Chambers, S. P., Caron, P. R., Murcko, M. A., and Wilson, K. P. (1996) Structure and Mechanism of Inosine Monophosphate Dehydrogenase in Complex with the Immunosuppressant Mycophenolic Acid. *Cell* **85**, 921-930

48. Calise, S. J., Carcamo, W. C., Krueger, C., Yin, J. D., Purich, D. L., and Chan, E. K. L. (2014) Glutamine deprivation initiates reversible assembly of mammalian rods and rings. *Cellular and Molecular Life Sciences* **71**, 2963-2973

49. Toth, E. A., and Yeates, T. O. (2000) The structure of adenylosuccinate lyase, an enzyme with dual activity in the *de novo* purine biosynthetic pathway. *Structure* **8**, 163-174

50. Altman, B. J., Stine, Z. E., and Dang, C. V. (2016) From Krebs to clinic: glutamine metabolism to cancer therapy. *Nature Reviews Cancer* **16**, 619-634

51. de Cima, S., Polo, L. M., Diez-Fernandez, Martinez, A. I., Cervera, J., Fita, I., and Rubio, V. (2015) Structure of human caramoyl phosphate synthetase: deciphering the on/off switch of human ureagenesis. *Scientific Reports* **5**

52. Liao, L.-X., Song, X.-M., Wang, L.-C., Lv, H.-N., Chen, J.-F., Liu, D., Fu, G., Zhao, M.-B., Jiang, Y., Zeng, K.-W., and Tu, P.-F. (2017) Highly selective inhibition of IMPDH2 provides the basis of antineuroinflammation therapy. *PNAS* **114**, E5986-E5994

53. Scott, J. W., Hawley, S. A., Green, K. A., Anis, M., Stewart, G., Scullion, G. A., Norman, D. G., and Hardie, D. G. (2004) CBS domains form energy-sensing modules whose binding of adenosine ligands is disrupted by disease mutations. *The Journal of Clinical Investigation* **113**, 274-284

54. Buey, R. M., Ledesma-Amaro, R., Velazquez-Campoy, A., Balsera, M., Chagoyen, M., de Pereda, J. M., and Revuelta, J. L. (2015) Guanine nucleotide binding to the Bateman domain mediates the allosteric inhibition of eukaryotic IMP dehydrogenases. *Nature Communications* **6**

55. Buey, R. M., Fernandez-Justel, D., Marcos-Alcalde, I., Winter, G., Gomez-Puertas, P., de Pereda, J. M., and Revuelta, J. L. (2017) A nucelotide-controlled conformational switch modulates the activity of eukaryotic IMP dehydrogenases. *Scientific Reports* **7**

56. Labesse, G., Alexandre, T., Vaupre, L., Salard-Arnaud, I., Him, J., Lai Kee, Raynal, B., Bron, P., and Munier-Lehmann, H. (2013) MgATP Regulates Allostery and Fiber Formation in IMPDHs. *Structure* **21**, 975-985

57. Labesse, G., Alexandre, T., Gelin, M., Haouz, A., and Munier-Lehmann, H. (2015) Crystallographic studies of two variants of *Pseudomonas aeruginosa* IMPDH with impaired allosteric regulation. *Acta Cryst.* **D71**, 1890-1899

58. Chang, C.-C., Lin, W.-C., Pai, L.-M., Lee, H.-S., Wu, S.-C., Ding, S.-T., Liu, J.-L., and Sung, L.-Y. (2015) Cytoophidium assembly reflects upregulation of IMPDH activity. *Journal of Cell Science* **128**, 3550-3555

59. Dierley Keppeke, G., Calise, S. J., Chan, E. K. L., and Andrade, L. E. C. (2015) Assembly of IMPDH2-based, CTPS-based, and Mixed Rod/Ring Structures Is Dependent on Cell Type and Conditions of Induction. *Journal of Genetics and Genomics* **42**, 287-299

60. Duong-Ly, K., Kuo, Y.-M., Johnson, M. C., Cote, J. M., Kollman, J. M., Soboloff, J., Rall, G. F., Andrews, A. J., and Peterson, J. R. (2018) T cell activation triggers reversible inosine-5'-monophosphate dehydrogenase assembly. *Journal of Cell Science* **131**

61. Keppeke, G. D., Calise, S. J., Chan, E. K. L., and Andrade, L. E. C. (2015) Assembly of IMPDH2-based, CTPS-based, and Mixed Rod/Ring Structures Is Dependent on Cell Type and Conditions of Induction. *Journal of Genetics and Genomics* **42**, 287-299

62. Keppeke, G. D., Chang, C. C., Peng, M., Chen, L.-Y., Lin, W.-C., Pai, L.-M., Andrade, L. E. C., Sung, L.-Y., and Liu, J.-L. (2018) IMP/GTP balance modulates cytoophidium assembly and IMPDH activity. *BMC Cell Division* **13**

63. Anthony, S. A., Burrell, A. L., Johnson, M. C., Duong-Ly, K., C., Kuo, Y.-M., Simonet, J. C., Michener, P., Andrews, A., Kollman, J. M., and Peterson, J. R. (2017)

Reconstituted IMPDH polymers accomodate both catalytically active and inactive conformations. *Molecular Biology of the Cell* **28**, 2600-2608

64. Thomas, E. C., Gunter, J. H., Webster, J. A., Schieber, N. L., Oorschot, V., Parton, R. G., and Whitehead, J. P. (2012) Different Characteristics and Nucleotide Binding Properties of Inosine Monophosphate Dehydrogenase (IMPDH) Isoforms. *PLoS ONE* **7**

65. John, C. S., Purich, D. L., Nguyen, T., Saleem, D. A., Krueger, C., Yin, J. D., and Chan, E. K. L. (2016) 'Rod and ring' formation from IMP dehydrogenase is regulated through the one-carbon metabolic pathway. *Journal of Cell Science* **129**, 3042-3052

66. O'Connell, J. D., Zhao, A., Ellington, A. D., and Marcotte, E. M. (2012) Dynamic Reorganization of Metabolic Enzymes into Intracellular Bodies. *Annual Review of Cell and Developmental Biology* **28**, 89-111

67. Ji, Y., Gu, J., Makhov, A. M., Griffith, J. D., and Mitchell, B. S. (2006) Regulation of the Interaction of Inosine Monophosphate Dehydrogenase with Mycophenolic Acid by GTP. *Journal of Biological Chemistry* **281**, 206-212

68. Keppeke, G. D., Calise, S. J., Chan, E. K. L., and Andrade, L. E. C. (2019) Ribavirin induces widespread accumulation of IMP dehydrogenase into rods/rings structures in multiple major mouse organs. *Antivirial Research* **162**, 130-135

69. Narayanaswamy, R., Levy, M., Tsechansky, M., Stovall, G. M., O'Connell, J. D., Mirrrielees, J., Ellington, A. D., and Marcotte, E. M. (2009) Widespread reorganization of metabolic enzymes into reversible assemblies upon nutrient starvation. *Proc. Natl. Acad. Sci.* **106**, 10147-10152

70. Aughey, G. N., and Liu, J.-L. (2017) Metabolic regulation via enzyme filamentation. *Critical Reviews in Biochemistry and Molecular Biology* **51**, 282-293

71. Carcamo, W. C., Satoh, M., Kasahara, H., Terada, N., Hamazaki, T., Chan, J. Y. F., Yao, B., Tamayo, S., Covini, G., von Muhlen, C. A., and Chan, E. K. L. (2011) Induction of Cytoplasmic Rods and Rings Structures by Inhibition of the CTP and GTP Synthetic Pathway in Mammalian Cells. *PLoS ONE* **6**

72. Lynch, E. M., Kicks, D. R., Shepherd, M., Endrizzi, J. A., Maker, A., Hansen, J. M., Barry, R. M., Gitai, Z., Baldwin, E. P., and Kollman, J. M. (2017) Human CTP synthase filament structure reveals the active enzyme conformation. *Nature Structure and Molecular Biology* **24**, 507-514

73. Noree, C., Monfort, E., Shiau, A. K., and Wilhelm, J. E. (2014) Common regulatory control of CTP synthase enzyme activity and filament formation. *Molecular Biology of the Cell* **25**, 2282-2290

74. Chang, C.-C., Keppeke, G. D., Sung, L.-Y., and Liu, J.-L. (2018) Interfilament interaction between IMPDH and CTPS cytoophidia. *The FEBS Journal* **285**, 3753-3768

75. Schmitt, D. L., and An, S. (2017) Spatial Organization of Metabolic Enzyme Complexes in Cells. *Biochemistry* **56**, 3184-3196

76. Zhang, S., Ding, K., Shen, Q.-J., Zhao, S., and Liu, J.-L. (2018) Filamentation of asparagine synthetase in *Saccharomyces cerevisiae*. *PLoS Genetics* **14**

77. Chiang, K.-M., Yang, H.-C., and Pan, W.-H. (2018) A Two-Stage Whole-Genome Gene Expression Association Study of Young-Onset Hypertension in Han Chinese Population of Taiwan. *Scientific Reports* **8**

78. Arking, D. E. et. al. (2014) Genetic association study of QT interval highlights role for calcium signaling pathways in myocardial repolarization. *Nature Genetics* **46**, 826-836

79. Dierley Keppeke, G., Andrade, L. E. C., Grieshaber, S. S., and Chan, E. K. L. (2015) Microinjection of specific anti-IMPDH2 antibodies induces disassembly of cytoplasmic rods/rings that are primarily stationary and stable structures. *Cell and Bioscience* **5**

80. Labesse, G., Alexandre, T., Vaupre, L., Salard-Arnaud, I., Lai Kee Him, J., Raynal, B., Bron, P., and Munier-Lehmann. (2013) MgATP Regulates Allostery and Fiber Formation in IMPDHs. *Structure* **21**, 975-985

81. Guo, K.-M., Chang, C.-C., Shen, Q.-J., Sung, L.-Y., and Liu, J.-L. (2014) CTP synthase forms cytoophidia in the cytoplasm and nucleus. *Experimental Cell Research* **323**, 242-253

82. Liu, J.-L. (2010) Intracellular compartmentation of CTP synthase in *Drosophila Journal of Genetics and Genomics* **37**, 281-296

83. Yang, H., Ralle, M., Wolfgang, M. J., Dhawan, N., Burkhead, J. L., Rodriguez, S., Kaplan, J. H., Wong, G. W., Haughey, N., and Lutsenko, S. (2018) Copper-dependent amino oxidase 3 governs selection of metabolic fuels in adipocytes. *PLoS Biology* **16**

84. Stein, L. R., and Imai, S.-i. (2012) The dynamic regulation of NAD metabolism in mitochondria. *Trends in Endocrinology and Metabolism* **23**, 420-428

Curriculum Vitae

The Johns Hopkins University School of Medicine

Dawn Hayward April 5th, 2019

Educational History:

Ph.D. expected 2019 Program in Biochemistry, Johns Hopkins School of Medicine
Cellular and Molecular Biology
Mentor: Svetlana Lutsenko, PhD

B.S 2013 Biochemistry Temple University

Other Professional Experience:

Science Writer 2016-2019 The American Society of Biochemistry and Molecular Biology Today Magazine

Science Writer 2017-2017 The Chemical & Engineering News Media Group

Scholarships, fellowships, or other external funding:

NIH F31 NRSA 3/15/2016-8/31/2017
Award number: 1F31GM117940-01A1
Sponsor: Philip Cole, MD, PhD

Publications, peer reviewed

Wu M, **Hayward D**, Kalin JH, Song Y, Schwabe JW, Cole PA (2018) Lysine-14 acetylation of histone H3 in chromatin confers resistance to the deacetylase and demethylase activities of an epigenetics silencing complex. Elife 7:e37231. PMCID: PMC6019071.

Kalin JH, Wu M, Gomez AV, Song Y, Das J, **Hayward D**, Adejola N, Wu M, Panova I, Chug HJ, Kim E, Roberts HJ, Roberts JM, Prusevich P, Jeliazhov JR, Burman SSR, Fairall L, Milano C, Eroglu A, Proby CM, Dinkova-Kostova AT, Hancock WW, Gray JJ, Bradner JE, Valenta S, Mai A, Anders NM, Rudek MA, Hu Y, Ryu B, Schwabe JWR, Mattevi A, Alani RM, Cole PA (2018) Targetign the CoREST complex with dual histone deacetylase and demethylase inhibitors. Nature Communications 9:53. PMCID: PMC5754352.

Chen Z, Dempsey DR, Thomas SN, **Hayward D**, Bolduc DM, Cole PA (2016) Molecular Features of Phosphatase and Tensin Homolog (PTEN) Regulation by C-terminal

Phosphorylation. 291 (27): 14160-14169. PMCID: PMC4933174.

Publications, chapters and other non-peer reviewed:

Hayward D, Kouznetsova V, Pierson H, Hasan NM, Tsigelny I, Lutsenko S (2019) ANKRD9 is
a metabolically-controlled regulator of IMPDH2 abundance and macro-assembly. *Submitted*

Hayward D, Cole PA (2016) LSD1 Histone Demethylase Assays and Inhibition. Methods in Enzymology 573: 261-278. PMCID: PMC5178825

Posters and abstracts:

Wu M, **Hayward D**, Kalin JH, Song Y, Schwabe J, Cole PA (2018) Analysis of CoREST Complex-Chromatin Interactions with Chemical Tools. Federation of American Societies for Experimental Biology Meeting, San Diego CA, April 21-25, 2018

Hayward D, Hasan N, Chang D, Pierson H, Lutsenko S (2017) The Role of ANKRD9 in protein compartmentalization and copper homeostasis. Program in Biochemistry, Cellular and Molecular Biology Annual Retreat, St. Michaels MD, October 7-9, 2017

Wu M, **Hayward D**, Kalin JH, Song, Y, Schwabe JWR, Cole PA (2017) Chemical Tools to Study the Molecular Mechanisms of the CoREST Complex-Chromatin Interactions. Federation of American Societies for Experimental Biology Meeting, Chicago IL, April 22-26, 2017

Kalin J, Wu M, **Hayward D**, Wang L, Roberts, J, Prusevich P, Hancock W, Bradner J, Ryu B, Alani R, Cole P (2015) CoREST in Peace: Dual Action Inhibitors of Histone Deacetylase and Lysine Specific Demethylase. Federation of American Societies for Experimental Biology Meeting, Boston MA, April 2-5, 2015